Thiourea-urea metal (Cd & Ni) chalcogenide (O & S) complexes for the synthesis and characterization of metal chalcogenide nanoparticles

By

Student Name: Mr TANKISO MASANGANE

Student Number: 209060832

The Dissertation submitted for the fulfillment of the requirements for the degree of

MAGISTER TECHNOLOGIAE

Faculty of Applied and Computer Science

Department of Chemistry

Vaal University of Technology

SUPERVISOR: Prof M.J MOLOTO

CO-SUPERVISOR: Dr T XABA

DECLARATION STATEMENT

"I hereby declare that the work on thiourea-urea metal dichalcogenide complexes for the synthesis and characterization of metal chalcogenide nanoparticles is a presentation of my original research work. Wherever contributions of others are involved, every effort is made to indicate this clearly, with due reference to the literature, and acknowledgment of collaborative research and discussion.

The work was done under the supervision of Professor M.J Moloto at the Vaal University of Technology.

T.J MASANGANE:…….. Date: …….

SUPERVISOR: …… Date:……...

ACKNOWLEDGEMENTS

I would like to thank all the people who contributed to the work described in this dissertation. First and foremost, I would like to gratefully and sincerely thank my supervisor, Professor M.J Moloto, for accepting me into his research group and for all the support and encouragement he gave me during the long months I spent undertaking my field of work at the Vaal University of Technology. I would like to thank him for allowing me to grow as a research scientist. His advice on my career has been invaluable, engaging me in new ideas, and demanding a high quality of work in all my endeavors. Without his guidance and constant feedback, this degree would not have been achievable.

My gratitude also goes to the department of chemistry at the Vaal University of Technology, for giving me the opportunity to study at the institution, especially the members of NCAP group for their input, valuable discussions, and accessibility. The group has been a source of friendships as well as good advice and collaboration. I would like to acknowledge honorary group members Dr. Pierre Mubiayi and Dr. Pardon Nyamukamba for making effort to keep the group meetings running accordingly. My appreciation also goes to Wits University, University of Johannesburg, University of Cape Town and Mintek for their assistance in analytical instrumentations. I would also like to acknowledge National Research Foundation (NRF) for their financial support.

I would like to acknowledge friends and family who supported me during my time of the study. First and foremost I would like to thank my parents for shaping me to be individual that I am today. My loving siblings, Sithole, Mmatlala, Dikeledi, Mmatluwa and Sello. My ecstatic

nephews, Refilwe, Palesa, Malefu, Lebohang, Qhayiya and Kamohelo. I have been extremely fortunate in my life to have family that has shown me love and support. My heart taking gratitude goes to my girlfriend Nthabiseng Rankoetseng for her overwhelming support and nudge for me to achieve my goals as she was the source of inspiration for me.

Finally, I would like to acknowledge friends, Snyman Modise, Ronnie Sebetlele, Matsemela Motsoeneng, Themba Ntuli and Wanda Bout. I would also like to give special thanks to T Mofokeng and K Mnqiwu, Thanks guys for the encouragement and your persuasion for those late night study, it is literally true that this dissertation could not have been completed without your participation. I will also like to give thanks to everyone one that has touched my life one way or another, and, God He's the only reason I made it this far.

TABLE OF CONTENTS

TITLE PAGE…….

DECLARATION STATEMENT…….. (i)

ACKNOWLEDGEMENTS……...…….....… (ii)

TABLE OF CONTENT……. (v)

LIST OF FIGURES……..……..... (ix)

LIST OF TABLES……. (xii)

LIST OF ABBREVIATIONS…….…….. (xii)

ABSTRACT……...…….. (xv)

CHAPTER 01

INTRODUCTION

1.1 Nanoparticles.....2

1.1.1 Semiconducting nanoparticles 2

1.1.2 Quantum Dots..... 3

1.1.3 Cadmium Chalcogenides and Nickel chalcogenides nanoparticles..... 5

1.2 Synthesis 7

1.2.1 Colloidal method 8

1.2.2 Hydrothermal and Solvothermal methods 10

1.2.3 Single source precursor method..... 12

1.3 Applications.....14

1.3.1 Biological applications 15

1.3.2 Solar Cells..... 17

1.4 Aim, Objectives and Problem Statement.....19

1.4.1 Aim **19**

1.4.2 Objectives **19**

1.4.3 Problem statement..... **19**

Chapter 02

Literature review

2.1 Ligands.....22

2.1.1 Thiourea and urea ligands **22**

2.1.2 Metal chalcogenides complexes..... **24**

Chapter 03

Synthesis and characterization of metal chalcogenides, and dichalcogenides complexes

3.1 Chemical reagents.....27

3.2 Instrumentation 27

3.2.1 FT-IR Spectroscopy **27**

3.2.2 CHNS Elemental analysis..... **27**

3.2.3 Thermogravimetric analysis..... **27**

3.3 Preparation of the complexes..... **27**

3.3.1 Synthesis of cadmium chalcogenides complexes **28**

(a) Bis (thiourea) cadmium chloride.....28

(b) Bis (urea) cadmium chloride 29

(c) Bis (thiourea) cadmium chloride* 29

3.3.2 Synthesis of nickel chalcogenides complexes **30**

(a) Nickel thiourea.....30

(b) Nickel urea 30

(c) Nickel thiourea* 30

3.4 Results and Discussion.....31

3.4.1 FTIR spectral analysis of thiourea, urea, and their cadmium chalcogenides and dichalcogenide complexes.....**31**

(a) Thiourea and its cadmium complex.....32

(b) Urea and its cadmium complex.....33

(c) Cadmium urea, cadmium thiourea and cadmium thiourea*.....34

3.4.2 FTIR spectral analysis of thiourea, urea and their nickel chalcogenide and dichalcogenide complexes.....**36**

(a) FIR spectra of urea and nickel urea complex.....36

(b) FIR spectra of thiourea and nickel thiourea complex.....37

(c) FIR spectra of nickel thiourea, Nickel thiourea*.....38

3.4.3 Thermogravimetric analysis for complexes.....**39**

(a) TGA analysis of cadmium urea and cadmium thiourea complexes.....39

(b) TGA analysis of nickel urea and nickel thiourea complexes.....40

(c) TGA analysis of nickel thiourea*.....41

(d) TGA analysis of cadmium thiourea* and cadmium urea**.....42

3.4.4 Summary of results.....**44**

Chapter 04

Synthesis and characterization of metal chalcogenide nanoparticles from thiourea and urea-based cadmium and nickel complexes

4.1 Chemical reagents.....46

4.2 Instrumentation.....46

4.2.1 Optical properties.....**46**

4.2.2 X-ray diffraction analysis.....**46**

4.2.3 Electron microscopy.....**46**

4.3 Synthesis of cadmium and nickel chalcogenide nanoparticles.....46

4.4 Results and Discussion.....48

4.4.1 CdS and CdO nanoparticles from Cd-thiourea, complex 1 and Cd-urea.....**48**

(a) Qualitative analysis and optical properties of CdS nanoparticles.....48

(b) Structural properties of CdS nanoparticles.....51

(c) Optical properties of CdO nanoparticles. 54
(d) CdO nanoparticles structural properties 56
4.4.2 NiS and NiO nanoparticles from Ni-thiourea, nickel thiourea* and Ni-urea 57
(a) NiO nanoparticles Optical properties 57
(b) NiO nanoparticles structural properties 58
(c) Qualitative analysis and optical properties of NiS nanoparticles 60
(d) NiS nanoparticles structural properties 62

Chapter 05

Overall conclusion and recommendations

5.1 Conclusion 67

5.2 Recommendations for future work 69

LIST OF FIGURES

Figure 1.1: The spatial electronic state diagram showing the quantum confinement effect in bulk semiconductor and nanoparticles 3

Figure 2.1: Chemical structures of thiourea and urea. 21

Figure 2.2: Reaction equation of Zinc sulfate with thiourea and urea. 24

Figure 3.1: Diagram for the synthesis of complexes……..... 28

Figure 3.2: Infrared spectra of thiourea (b) and its cadmium complex (a). 33

Figure 3.3: Infrared spectra of urea and its cadmium complex. 34

Figure 3.4: FTIR Spectra of cadmium thiourea, cadmium urea, and cadmium thiourea*. 35

Figure 3.5: FTIR spectra of urea (a) and its nickel complex (b)....36

Figure 3.6: FTIR spectra of thiourea ligand (a) and its nickel complex. 37

Figure 3.7: FTIR of nickel thiourea and nickel thiourea*. 38

Figure 3.8: TGA profile of cadmium thiourea and cadmium urea. 40

Figure 3 9: TGA profile of nickel urea and nickel thiourea 41

Figure 3.10: TGA profile of (a) nickel urea and (b) nickel thiourea 42

Figure 3.11: TGA profile of thiourea-urea nickel. 43

Figure 4.1: X-ray photoelectron spectrum of CdS nanoparticles from cadmium thiourea*....48

Figure 4.2: CdS absorption spectra from cadmium thiourea and cadmium thiourea*. 51

Figure 4.3: CdS emission spectra of CdS from cadmium thiourea and cadmium thiourea*...51

Figure 4.4: The XRD pattern of CdS nanoparticles from cadmium thiourea. 52

Figure 4.5: The XRD pattern of CdS nanoparticles from cadmium thiourea*. 52

Figure 4.6: The TEM image of CdS nanoparticles from cadmium thiourea …..…….53

Figure 4.7: The TEM image of CdS nanoparticles from cadmium thiourea*. 53

Figure 4.8: Absorption spectrum of CdO nanoparticles. 55

Figure 4.9 Emission spectrum of CdO nanoparticles. 55

Figure 4.10 Histogram of CdO nanoparticles …….....56

Figure 4.11 TEM image of CdO nanoparticles ……...…...56

Figure 4.12 XRD pattern of CdO nanoparticles …….…… ……57

Figure 4.13 UV-Vis and PL spectra of NiO nanoparticles ……..…….. 58

Figure 4.14: Talc plot for NiO Nanoparticles. 58

Figure 4.15: TEM image of NiO nanoparticles 60

Figure 4.16: Histogram of NiO nanoparticles.....60

Figure 4.17: XRD pattern of NiO nanoparticles 61

Figure 4.18: The UV-Vis and PL spectra of NiS Nanoparticles synthesized from nickel thiourea complex.....63

Figure 4.19: Talc plot of NiS Nanoparticles synthesized from nickel thiourea complex.....63

Figure 4.20: XRD Pattern of NiS nanoparticles from nickel thiourea complex. 64

Figure 3.18: TEM images of NiS nanoparticles from nickel thiourea complex. 64

Figure 3.19: X-ray photoelectron spectrum of nanoparticles from nickel thiourea*…….…..65

Figure 4.20: UV-vis and PL spectra of NiS nanoparticles from cadmium thiourea*.....66

Figure 4.21: Talc plot of NiS nanoparticles from nickel thiourea* 66

Figure 4.22: TEM image of NiS nanoparticles from nickel thiourea* 67

Figure 4.23: XRD patterns of NIS nanoparticles from nickel thiourea*. 67

LIST OF TABLES

Table 3.1: Table of all complexes synthesis on section 3.3…… 31

Table 4.1: Synthesized complexes, their reaction mode, and expected end products. 35

LIST OF ABBREVIATIONS

Chemical Reagents

TOP: Trioctylphosphine

HDA: Hexadecylamine

TOPO: Trioctylphosphine oxide

JCPDS: Joint committee on powder diffraction standards

QD's: Quantum dots

Eg: Band gap

LED's: Light emitting diodes

FT-IR: Fourier transformed infrared spectroscopy

NMR: Nuclear magnetic resonance spectroscopy

UV-VIS: Ultraviolet-visible spectroscopy

PL: Photoluminescence spectroscopy

TEM: Transmission electron microscopy

TGA: Thermogravimetric analysis

XPS: X-Ray photoelectron spectroscopy

XRD: X-ray diffraction spectroscopy

Symbols and Constants

Mmol: millimole

nm: Nanometer

a.u: Arbitrary units

cm: centimetre

°C: Degree Celsius

eV: Electron volts

E: Energy

h: Planck’s constant

v: Frequency

T: Temperature

t: Time

λ: Effective electron wavelength

ABSTRACT

The understanding of the fundamental properties and potential use of semiconductor materials in nanotechnology has stimulated the interest of many researchers. Coordination compounds containing ligands with chalcogenide atoms as donors have received considerable attention. Among these chalcogenide ligands, thiourea and urea have been extensively used previously to form single source precursors for the synthesis of group II–VI semiconductor nanoparticles. The synthesis and study of semiconductor nanocrystals has become a subject area of considerable research interest because they have potentially useful applications such as biomedical imaging, sensing, light-emitting diodes (LEDs), photovoltaics and displays.

In this work, special attention has been given to the synthesis and characterization of cadmium and nickel chalcogenides nanoparticles because of their interesting and unique optical properties, using a single source precursor method. The mixed chalcogenide sources are also explored for their complexes or simple reactions to produce semiconductor nanoparticles. The advantages of single molecular precursors over other existing methods for the synthesis of metal chalcogenide nanoparticles has proven to be a more efficient route for the synthesis of high-quality nanocrystals. Cadmium and nickel complexes of urea and thiourea were successfully synthesized by refluxing metal salts of cadmium and nickel with thiourea and urea at 30-40 °C for an hour and the complex mixture was cooled at room temperature. The synthesized complexes were washed with methanol and acetone to remove impurities and dried in air. All other complexes were synthesized using the same refluxing synthesis method mentioned above. The characterization of all complexes was done using Fourier-Transform infrared spectroscopy, thermogravimetric analysis and CARLO ERBA elemental analysis. Nickel thiourea and cadmium thiourea complexes were found to be coordinating with the center metal through a sulfur atom, and the urea complexes through an oxygen atom. This observation of the coordination of metals with ligands makes these complexes suitable for use as the single source precursor for the synthesis of metal chalcogenides nanoparticles. The six resulted

complexes from above synthesis are of cadmium sulphide, cadmium oxide, and nickel sulphide, nickel oxide. The TGA showed that all the complexes were stable at room temperature, as they decomposed around 200 °C, which makes these complexes suitable to be used for the synthesis of nanoparticles.

The synthesized complexes reported in this study were used as a single source molecular precursor in the preparation of cadmium oxide, cadmium sulfide, nickel oxide, and nickel sulfide nanoparticles. The precursors were thermalized under nitrogen gas while refluxing at 160 °C for 1 hour, using HDA as the capping agent and TOP was used as the solvent. Crystalline semiconducting nanoparticles were obtained as the end product for all complexes, the resulting nanoparticles were washed with acetone to remove any impurities. The UV-Vis spectra of all the nanoparticles were blue-shifted, with their PL spectra red-shifted from the maximum absorption peak due to change in size of particles from bulk to nano-size.

XRD pattern of CdS nanoparticles from Cd-thiourea suggested that a hexagonal phase of CdS was formed, and TEM analysis showed large particle sizes that were polydispersed with the dominance of cubic and rod shaped particles. The XRD patterns of CdS nanoparticles from cadmium thiourea and urea mixture showed the mixture of hexagonal and cubic phase nanoparticles with the predominance of cubic phase and its TEM images shows small particles size ranging from less than 50 nm, and the particles were polydispersed with the predominance of spherical nanoparticles. The XRD pattern of CdO nanoparticles showed the cubic phase nanoparticles with the existence of broad peaks indicating small particle size distribution. The TEM images of CdO nanoparticles confirmed the XRD data showing small particle size distribution with a size average of 6.8 nm.

The NiS nanoparticles synthesized from Ni-thiourea complex showed narrow peaks with hkl indices indicating hexagonal phase. Particles has no clear morphology due to the agglomeration of the nanoparticles that can be caused by the instability of the nanoparticles because of their high surface area. A cluster of particles can be observed from the TEM images, making it difficult to determine the particle size and shape of NiS particles from Ni-thiourea complex. NiS particles from nickel thiourea and urea mixture also showed XRD patterns of the hexagonal plane and TEM showed small size conjugated nanocrystals. The TEM of NiO indicated a spherical morphology, existence of other morphology rather than spherical can also be observed from the image. The average particle size was 8 nm, and XRD pattern showed the cubic phase of NiO nanocrystals.

CHAPTER ONE

Introduction

1.1 Nanoparticles

1.1.1 Semiconducting nanoparticles

A great deal of effort has been devoted to the research of nanocrystallites of semiconductors because of their quantum size effect and potential applications. The world of computing is revolutionizing as the electronic devices contain computer chips which are made from semiconductor materials are being used to make supercomputers. Semiconductors are defined as materials in which the valence band is filled with electrons and the unoccupied conduction band is separated by small band gap. When the electrons absorb enough thermal or optical energy, larger than their band gap, they are able to jump from the valence band to the conduction band. The difference between the microcrystalline semiconductor and the corresponding nanocrystalline material arises from two fundamental factors that are size-related between the conduction and valence bands, which are responsible for their unique optical, electrical and chemical properties. The band gap energy of the nanoparticles can simply be calculated from the equation:

$$E_g = hc/\lambda \qquad \textbf{(Equation 1.1)}$$

Where E_g is the band gap energy, h is the planks constant, c is the velocity of the light and λ is the absorption edge in reflectance spectra. The energy gap (E_g) from **(Figure 1.1)** separating the conduction and the valence energy band is influenced by the size of the particles.

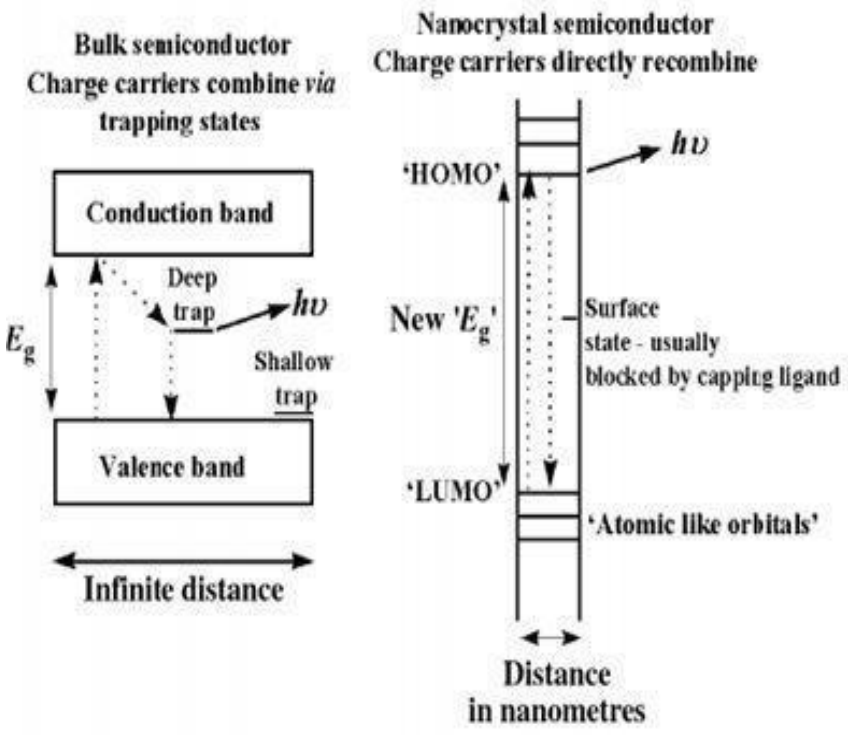

Figure 1.1: The spatial electronic state diagram showing the quantum confinement effect in bulk semiconductor and nanoparticles (Zhang et al., 2003)

The color emitted by semiconducting materials is determined by the band gap and particle-size. Quantum confinement generally refers to the widening of the HOMO-LUMO gap with a decrease in crystallite size. This effect is due to the electron being trapped thus giving rise to discrete energy level, rather than continuous band found in bulk materials. This results in the "electron and hole" produced by the absorption of a photon for semiconductor nanoparticles to be closer to each other than in macrocrystalline materials.

1.1.2 Quantum Dots

Semiconductor nanomaterials are also referred to as "quantum dots (QD's)" when their size range from 1nm to 20 nm. QD's consist of a few hundred thousand of atoms, whose radii are smaller than the bulk exciton Bohr radius. The exciton Bohr radius is a concept where excitons

have a natural physical separation between the electron and the hole which is dependent on the material. In QD's, the exciton Bohr radius is small compared to the size of the crystal, and the exciton is then relatively free to move around in the crystal. Quantum confinement of the electron and the hole in all three dimensions leads to an increase in the effective band gap of the material with a decrease in crystallite size. Consequently, both the optical absorption and emission of quantum dots shift to higher energies as the size of the dots become smaller. Recent advances in the synthesis of highly monodisperse nanocrystallites have paved the way for numerous spectroscopic studies assigning the QD's electronic states and mapping out their evolution as a function of size. The size and shape of QD's control their widely varying electrical and optical properties (Jorge *et al.*, 2007). One of the most active trends in modern materials chemistry is the development of synthetic routes to control the size and shape of semiconductor nanoparticles.

Semiconductor nanocrystals are also of great interest for both fundamental research and technical applications because of the large ratio of surface atoms to volume and the three-dimensional quantum confinement of excitons. One of the difficulties in synthesizing nanoparticles of 0D (spheres, cubes), 1D (rods, wires) and 2D (discs, prisms, plates) is the control of growth through variation of the critical parameters used to control the morphology of quantum dots. Some of these critical parameters includes temperature, concentration, reaction time, capping agent, solvent, pH, and precursor nature (N Moloto *et al.*, 2009). These parameters play an important role in the synthesis of the nanocrystals because the variation of these parameters affects the morphology of the nanoparticles. The choice of the synthetic

method also plays a vital role in the morphologies of the nanoparticles (Srinivasan, 2014). Basic research is leading to the development of true nanotechnologies which have the potential to impact fields of health care, data storage, sensing and electronics to energy and environment. The ultimate scientific and technological impact of these materials mainly depends on their novel electronic, optical, catalytic, physical, biological and chemical properties (Meyer and Korkekoulu, 2000). Hence, studies concerning quantum dots and electronic confinement observed in these semiconducting materials are of exceptional importance.

1.1.3 Cadmium Chalcogenides and Nickel chalcogenides nanoparticles

Cadmium chalcogenides and nickel chalcogenides nanomaterials are part of semiconductor nanomaterials attracting many researchers' attention. Cadmium oxide is a group II-VI and n-type semiconductor nanomaterial with a cubic structure and a direct bandgap of 2.3 eV and the indirect band gap of 1.98 eV. Cadmium oxide nanoparticles are attracting tremendous attention due to their interesting properties like direct band gap of 2.3 eV and the CdO semiconductors are almost entirely transparent in the optical region of the electromagnetic spectrum and have high conductivity. Interest in CdO over the past few years has been prompted by the optoelectrical devices operating at the short wavelength and thin-film photovoltaic and flat panel displays.

Among the family of group II-VI semiconductors, CdS is the foremost investigated because of the favorable electronic and optical properties for the optoelectronic application. CdS nanomaterials have already shown vital applications in fluorescence probe sensors, solar battery photo-electro catalysis, and laser light-emitting diodes. In recent years, effective

synthetic routes to produce CdS nanoparticles have been widely investigated. It is well known that the optical properties of the semiconductor nanoparticles depend on their size and crystallinity. Therefore, the preparation of high-quality CdS nanoparticles has a great influence on their optical properties. Moloto and Revaprasadu reported on CdS nanoparticles from the single source precursors by thermalizing the Cd(II) complexes of dithiocarbamate using a coordinating solvent such as hexadecylamine, tri-n-octylphosphine and tri-n-octylphosphine oxide (Revaprasadu and Mlondo, 2006). Different methodologies have been used to synthesize these nanomaterials but reported procedures have limited control on the particle functionality. It is an urgent need to modify cost-effective procedure in chemical and environment-friendly approach for the synthesis of nanomaterials.

Nickel sulfides nanoparticles with different phase and morphology such as layer-rolled NiS, cuboids, nanobelts, three-dimensional flowers like rhombohedral and dodecahedral NiS_2, have been synthesized using different methods. These NiS nanoparticles have potential applications in lithium ion batteries, supercapacitors, and dye-sensitized solar cells. NiS_2 is a p-type semiconductor with a band gap of 0.5 eV and it is potentially useful in the photoelectrochemical solar cell. Nickel sulfide has more complex phases such as NiS (α-NiS and β-NiS), Ni_3S_2, NiS_2, Ni_3S_4, Ni_9S_8, and Ni_7S_6 making the synthesis of single phase NiS complicated. Nickel sulfide shows two different phase types, depending on the synthesis temperature. Roffey and co-workers reported on the phase transformation of α-NiS to β-NiS occur at 250 ºC (Roffey *et al.*, 2016).

Several methods for the synthesis of nickel sulfide nanocrystal have been investigated. Solvothermal and wet chemical methods which involve high-temperature solid state and vapor phase reactions have been used to synthesize nickel chalcogenides nanoparticles. However controlled phase NiS is difficult to synthesize using these methods. The synthesis of NiS in a phase such as Ni_3S_4 requires a two-step reduction process to control the phase and morphology, Karthikeyan reported on shape controlled of sulfur based nickel nanocrystals by injecting a molecular precursor into high boiling point solvent. The use of oleylamine-metal complex has been well studied, and Thomson reported on the synthesis of various size controlled metal chalcogenides nanocrystals including NiS with particle size ranging between 6-13 nm (Karthikeyan *et al.*, 2015).

Non-stoichiometric Nickel oxide (NiO) is a good p-type semiconductor with a cubic lattice structure, owing to its structural defects, NiO has a potential use in a variety of applications such as catalysis, battery cathodes, gas sensors and magnetic materials (Barakat *et al.*, 2013). Nickel oxide exhibits anodic electrochromism excellent durability and electrochemical stability, large spin optical density and various manufacturing possibilities. Nanocrystals of NiO possess many improved properties than those of micrometer-sized NiO particles (Moloto, 2009). Nickel sulfide has also found plenty of applications such as in optical recording materials, solar cells, sensors, laser materials, conductivity field, and optical fibers (Wang *et al.*, 2014).

1.2 Synthesis

There are various methods reported for the synthesis of NiS nanoparticles, solvothermal is by far the most reported method (Jorge *et al.*, 2007). The single source precursor method has also

been reported for the synthesis of nickel sulfide thin film via the CVD method. The solvothermal method has resulted in the various morphologies such as star shape and octahedral nickel selenide (N. Moloto *et al.*, 2009). Semiconductor nanoparticles have been prepared by various synthesis. Chemical methods are the most used for the synthesis of nanomaterials due to their low cost, reliability and are environmentally friendly when compared to physical methods (Top-down approach). Chemical methods are versatile in synthesizing nanoparticles and feasible in controlling the particle shape and size distribution. These chemical synthesis methods include (I) colloidal method, (II) growth in confined matrices, (III) metal organic routes, (V) single source precursor method, (IV) hydrothermal synthesis etc, and many more. These techniques based on chemical approach have been developed for the synthesis of semiconductor nanoparticles with high purity, narrow size distribution, surface derivatized and monodispersed crystalline nanoparticles which are reasonably stabilized from the surrounding environment by a capping agent to preserve their properties (Malik *et al.*, 1997).

1.2.1 Colloidal method

The colloidal method is simple and well established wet chemistry technique which involves controlled precipitation processes in which dilute colloidal homogenous solution of the different ions are mixed under controlled temperature. Different ions are mixed under controlled temperature and pressure to form insoluble precipitates and the cessation of growth immediately after nucleation. The colloidal route is the first reported method used to synthesize such small particles (Mer, 2010). Semiconductor nanocrystals are synthesized from precursor compounds dissolved in solutions, much like the traditional chemical processes. The basic principle of colloidal preparation of nanoparticles was known since the ancient past like gold

colloidal used for high quality red and purple stained glass from medieval churches. However, proper scientific investigation of colloidal methods started in 1857 when Michael Faraday published results of his experiments with gold (Tweney, 2006). The synthesis of colloidal semiconductor nanocrystals is based on precursors, organic surfactants, solvents, and temperature. These features play an important role in determining the morphologies of the synthesized colloidal nanoparticles. The temperature during growth process is one of thecritical factors in determining optimal conditions for the nanocrystal growth. It must be high enough to allow for rearrangement and annealing of atoms during synthesis process while being low enough to promote crystal growth, these means one should set the temperature to the optimum to allow these processes to take place. Another critical factor that must be stringently controlled during nanocrystal growth is the monomer or precursor concentration. At high monomer concentrations, the critical size (the size where nanocrystals neither grow nor shrink) is relatively small, resulting in growth of nearly all particles. In this regime, smaller particles grow faster than large ones (since larger crystals need more atoms to grow than small crystals) resulting in "focusing" on the size distribution to yield nearly monodisperse particles. The size focusing is optimal when the monomer concentration is kept such that average nanocrystal size present is always slightly larger than the critical size.

When the monomer concentration is depleted during growth, the critical size becomes larger than the average size present, and the distribution "defocuses" proposed that if seeds (nuclei) could be made to grow into larger particles in a controlled manner, monodisperse particles could be formed (Mer, 2010). Further, if nucleation and growth are properly controlled,

particles with dimensions of the order of nanometres can be reproducibly synthesized. Nanocrystals, which are less stable in a solution, dissolve and then recrystallize on larger ones that are more stable. This process is called “Ostwald ripening”. For this process to be effective nanocrystals must have low solubility, which can be achieved by correct choice of solvent, pH, temperature and capping agent. High quality monodispersed particles are obtained when the processes of nucleation and growth are distinctly separated in a way that nucleation happens fast and growth take place slower. Significant contribution to this method was made by (Poznyak *et al.*, 2004). For the preparation of CdS nanoparticles, which involves the reaction of an aqueous solution of $CdSO_4$ and $(NH_4)_2S$ with particles size controlled by altering the nucleation kinetics by control of pH. Advantages of employing this method are that large batches of quantum dots may be synthesized. However, this method cannot be employed for synthesis of semiconductors like CdSe, GaAs, INP, and InAs. The instability of colloids at low temperatures make annealing of the particles difficult, which leads to poor crystalline materials being formed.

1.2.2 Hydrothermal and Solvothermal methods

Hydrothermal and solvothermal are an alternative approach to the use of high-temperature solvents, which can be both toxic and expensive. In a sealed vessel (bomb, autoclave, etc.), solvents can be brought to temperatures well above their boiling points by increase in the autogenous pressures resulting from heat. Performing a chemical reaction under such conditions is referred to as solvothermal processing or, in the case of using water as a solvent; the method is called hydrothermal processing. Solvothermal reaction conditions are extensively used in the preparation of inorganic solids, especially zeolites and hydrothermal

synthesis is a common method also used to synthesize zeolite/molecular sieve crystals. The hydrothermal method exploits the solubility of almost all inorganic substances in water at elevated temperatures and pressures and subsequent crystallization of the dissolved material from the fluid. Water at elevated temperatures plays an essential role in the precursor material transformation because the vapor pressure is much higher. Under the hydrothermal condition, a broad range of nanomaterial's and nanotubes with high-quality can be produced. During the synthesis of nanocrystals, parameters such as water pressure, temperature, reaction time, and the respective precursor, they can be tuned to maintain a high simultaneous nucleation rate and good size distribution. Solvothermal processes involve supercritical solvents. But most however indeed, simply take advantage of the increased solubility and reactivity of metal salts and complexes at elevated temperatures and pressures without bringing the solvent to its critical point. In any event, solvothermal processing allows many inorganic materials to be prepared at temperatures substantially below those required by traditional solid-state reactions. Unlike the cases of co-precipitation and sol-gel methods, which also allow for substantially reduced reaction temperatures, the products of solvothermal and hydrothermal reactions are usually crystalline and do not require post-annealing treatments. As a matter of safety, the pressures generated in a sealed vessel should always be estimated beforehand. Cushing and co-workers reported on the preparation of anatase by hydrothermally processing of hydrous titanium oxide prepared by the controlled hydrolysis of Ti $(OEt)_4$ in ethanol (Cushing, Kolesnichenko and O'Connor, 2004).

Jun and co-workers reported on the wurtzite ZnSe nanoparticles with sizes in the 18 nm range, starting from the Zinc and selenium precursors in ethylenediamine (en), this reaction yields a complex with the formula ZnSe (en). Nanoparticles of TiO_2, $LaCrO_3$, ZrO_2, $BaTiO_3$, $SrTiO_3$, $Y_2Si_2O_7$, Sb_2S_3, CrN, SnS_2, PbS, Ni_2P, and SnS_2 nanotubes, Bi_2S_3 nanorods, and SiC nanowires have been successfully synthesized in this way (Jun, Jung and Cheon, 2002). The solvent is not limited to water but also includes other polar or nonpolar solvents, such as benzene and the process is more appropriately called a solvothermal synthesis.

1.2.3 Single source precursor method

Considering that the ideal method should give pure, monodisperse, crystalline particles that are stabilized from the surrounding chemical environment by a capping agent. Ramasamy and co-workers reported on the precursor method which became popular for the preparation of high quality, crystalline, and monodispersed nanoparticles (Ramasamy *et al.*, 2010). He used this method to overcome the critical and hazardous conditions that are involved with other previously described methods like colloidal route by making use of organometallic and/or metal organic compounds under anaerobic conditions. A single source precursor method involves the decomposition of molecular precursor like cadmium thiourea or cadmium urea to produce a desired product. The advantage of single-source precursor method is that the bond between the metal and the chalcogenide already exist and the decomposition of the precursor under the right reaction conditions will results in the formation of metal chalcogenides nanoparticles for example. This approach has been used to produce various metal chalcogenides nanoparticles. Some of the examples of high quality, monodisperse crystalline

nanoparticles that were prepared by this route include CdSe, CdS, and CdTe (Revaprasadu and Mlondo, 2006).

The preparation of CdSe was achieved by using a hazardous metal alkyl (dimethyl cadmium) and a chalcogen source TOPSe (tri-n-octylphosphine selenide oxide) which is a polar coordinating Lewis base solvent. Although this method was found to produce highly monodispersed particles, which is one of the main requirements of semiconductor quantum dots. The use of dimethyl cadmium still posed some danger because of its hazardous status, especially at high temperature. To avoid this problem, single source precursor method was introduced to produce nanoparticles. These methods consist of a single compound containing all elements required within the synthesis of nanocrystallite. It was used to synthesize TOPO and HDA capped semiconductor nanoparticles like CdSe, CdS, NiS, NiSe and much more. In short, there are several potential advantages of using single-source/molecular precursors over other existing routes.

All precursor synthesis is carried out under anaerobic conditions, with the resulting precursors being air and moisture stable. In this work, the single source precursor method is over other methods due to its significant advantages compared to other methods as it was previously used and reported by Ramasamy as an efficient route to high-quality crystalline mono-dispersed nanoparticles (Ramasamy *et al.*, 2010). This method has opened a friendly way for the controllable synthesis of metal chalcogenides, it offers the distinct advantages of mildness, safety, and simplicity of fabrication procedure and equipment as compared to other methods. Other potential advantages of this method over other existing methods include, low-

temperature deposition route. The single source molecular precursor is also considered as a facile approach since it avoids problems of the use of environmental toxic organometallic materials by the use of environmental friendly materials. In a single source, a molecular precursor, the metal is already bonded to chalcogenide. Among various semiconductor materials, cadmium chalcogenides and nickel chalcogenides have been extensively investigated and used as an important direct band semiconductor, for the photoelectric conversion in solar cells, light-emitting diodes for a flat-panel display, and other optical devices based on its nonlinear properties Revaprasadu and Mlondo also reported the synthesis of various metal chalcogenide nanoparticles using single source precursor method (Revaprasadu and Mlondo, 2006). Thiourea and thiosemicarbazide complexes of cadmium and zinc were also used by Nair and Survase as the single source precursor for the synthesis of CdS, CdO and ZnS nanoparticles (Nair and Survase, 2014).

1.3 Applications

There is massive potential in the field of nanotechnology that transcends the conventional boundaries of biology, chemistry, and physics. This means nanotechnology has the possibility of having a huge impact on our everyday lives. Nanomaterials unique properties compared to bulk materials allows these nanomaterials to have several lifetime useful properties such as (mechanical, magnetic, electrical, optical, etc.), these properties can be selectively controlled by engineering the size, shape, and composition of the particles. There had already been exploitation of products of nanomaterial, but the products were previously not known that are within the nanoscale, since centuries ago there was no such advanced technology we have today to analyze or characterize such small particles. Alongside these products that have considerable

sales value, there are many novel products, which are currently available from a range of new companies and generally started from work originating from research studies at universities. Engineered nanomaterials are materials which have been designed and manufactured by human. These have been synthesized for a specific purpose and may be found in one of the several different shapes. As defined above, the term nano describes the size in at least one dimension so nanomaterials may have nano characteristics in 1D, 2D or 3D. These correspond to platelet-like, wire-like and spheroidal structures respectively.

The engineered nanomaterials may be further subdivided into organic and inorganic types, including carbon itself with specific nano characteristics. Inorganics include metals, and metalloid oxides, clays and a specific subset of compounds known as quantum dots and this variety of morphologies of the nanoparticles allows them to have different real-life applications.

1.3.1 Biological applications

Nanotechnology provides the tools to measure and understand bio-systems. Applications of nanomaterials in biomedicine, biotechnology, and agriculture include biocompatible implants, manipulation of molecules within cells, biocompatible electronic devices and ‘‘smart’’ controlled release delivery of drugs to the bio-system. Nano-oncology offers fascinating promises in cancer treatment with the potential for delivery of anticancer drugs and the localized killing of cancerous and precancerous cells or for more general drug delivery with some potential for drug delivery across the blood–brain barrier. Recently, researchers

conducted an animal study which showed that nanoparticles could be used to map a lymph node nearest a breast cancer. Inactivated drug can be attached to nanoparticles and once they reach a tumor they can be activated by a flash of light. Researchers at Washington University School of Medicine in St. Louis have also shown that nanoparticles carrying a toxin found in the bee venom can destroy human immunodeficiency virus (HIV) while leaving surround cells unharmed. All these findings which most of them are still under research around the world can lead to the world that is free from sickness like HIV, Cancer etc. The development of delivery systems for small molecules, proteins, and DNA to the bio-system has been impacted to an enormous degree over the past decade by nanotechnology and has led to the development of entirely new and unpredicted fields in biotechnology.

For the pharmaceutical industry, novel drug delivery technologies represent a strategic tool for expanding drug markets. The technology can address issues associated with current pharmaceuticals such as extending product life (line extension) or can add to their performance and acceptability, either by increasing efficacy or improving safety and patient compliance. In addition, the newer drugs developed with the help of computational chemistry using the knowledge gained from the human genome project require drug delivery systems for their effective use. This technology permits the delivery of drugs that are highly water-insoluble or unstable in the biological environment. It is expected that novel drug delivery systems can make a significant contribution to global pharmaceutical sales. This is illustrated by the fact that approximately 13% of the current global pharmaceutical market is accounted for by sales of products incorporating a drug delivery system. In recent years, many new pharmaceutical

companies have been established that can provide expertise in innovative delivery technology. Also, many established pharmaceutical industries are gearing up their efforts towards developing more effective and performance-based new drug delivery systems. Future work in this area includes the introduction of QDs in beads which are being inserted into the body to target infected cells. Near-infrared (NIR) quantum dots are showing promise in the biomedical imaging of living tissue because nanocrystals emitting in this region (700-1000 nm) possess well known optical transparency in biological tissues (Sahoo and Labhasetwar, 2003).

1.3.2 Solar Cells

QDs have the potential to increase the capabilities of solar cells that are currently in use today. It is well known that current energy sources are beginning to run out and alternatives sources of energy need to be found. Photovoltaic (PV) solar cells are one of the sources aiming to convert solar energy to electricity. Current research is trying to increase the efficiency of this conversion, which currently needs a large surface area and only a small percentage of light captured is converted. the currently used material is amorphous silicon (Jorge *et al.*, 2007). The problem with silicon is that it must be of very high purity and have a near perfect crystal structure and this process is very expensive, whereas the efficiency of such cells is very small, only converting about 13-18% of sunlight to electricity.

Quantum dots have the potential to increase the efficiency and reduce the cost of currently used typical silicon photovoltaic cells. Quantum dots of lead selenide can produce as many as seven excitons from one high energy photon of sunlight (7.8 times the band gap energy). This compares to silicon photovoltaic cells which can only manage one exciton per high energy

photon, with high kinetic energy carriers losing their energy as heat. This would result in a 7-fold increase in final output and also boost the maximum theoretical efficiency from 31% to 42%. Quantum dot photovoltaic would theoretical be cheaper to manufacture, as they can be made using simple chemical reactions used in the laboratory on a larger scale. The generation of more than one exciton by a single photon is called multiple exciton generations (MEG) or carrier multiplication. The high efficiency of the nanomaterials semiconductors is due to their larger surface area to volume ratio. Other materials that have been investigated for the use as the photoelectrical solar cell is titanium dioxide nanoparticles, the material has optical transparency, excellent stability, and good electrical conductivity. The benefit of this materials compared to silicon is that it can be fabricated from low purity materials by simple and low-cost procedures. In the current work on semiconductors nanomaterials for application in a solar cell, new devices or other semiconducting nanomaterials have been investigated because of their size-tunable band gaps due to size quantization and there is a promise that more efficiency solar cells can be produced for electricity production and hydrogen production processes.

1.4 Aim, Objectives and Problem Statement

1.4.1 Aim

The aim of this research was to synthesize and characterize metal chalcogenide nanoparticles from nickel and cadmium, chalcogenide and dichalcogenide complexes.

1.4.2 Objectives

- To synthesize metal chalcogenide and dichalcogenide complexes, from nickel and cadmium salt metal sources.
- Characterization of the complexes using elemental analysis (EL), Fourier Transform Infrared (FTIR) spectroscopy, and thermogravimetric analysis (TGA).
- Synthesize of cadmium chalcogenide and nickel chalcogenide nanoparticles, using single source precursor method.
- Characterization of the metal chalcogenide nanoparticles and by using Ultraviolet-Visible spectroscopy (UV-VIS), Photoluminescence spectroscopy (PL), Transmission Electron Microscopy (TEM), Powder X-ray Diffraction (PXRD) and X-ray photoelectron spectroscopy (XPS).

1.4.3 Problem statement

An ideal method for the synthesis of nanoparticles is one that gives pure, monodisperse, crystalline nanoparticles with controlled shape and size and they should be stabilized from the surrounding chemical environment by a capping agent to prevent agglomeration. Various new methods have been developed for the synthesis of nanoparticles because previously used

methods had limitations like use of hazardous and toxic chemicals at high temperature, use of costly and time-consuming methods (Morifi., 2014). One of the recently developed methods is single source precursor method, this method has been favored by many researchers because of its simplicity, it uses single source precursors that already have bond of interest between the metal and the chalcogenide ligand and the simple thermolysis of this precursor produces semiconducting nanoparticles (O'Brien et al., 2001). This method involves the preparation of the metal complexes first, which are then used as the source of metal chalcogenide nanoparticles. Metal chalcogenide complexes are the mostly widely used complexes for the synthesis of nanoparticles. There is less work reported on the use of metal dichalcogenide complexes for the synthesis and study of metal chalcogenides nanoparticles.

Chapter 02

Literature Review

2.1 Ligands

2.1.1 Thiourea and urea ligands

Thiourea is an interesting hybrid ligand with both hard (nitrogen) and soft (sulphur) donor atoms, hence it has the ability to act as an unidentate ligand forming strong metal chalcogenides complexes with both group IB and IIB metal ions, particularly Cu(II), Ag(I), Au(II) and Hg(II). Thiourea reduces Cu(II) to Cu(I), Au(II) to Au(I), Pt(IV) to Pt(II) and Te(IV) to Te(II), and it forms complexes with the metals in the lower oxidation state, hence the claim that thiourea stabilizes Rh(IV) in the solution is surprising, and the only metal reported to be N-bonded to the thiourea is Ti(IV), all other are S-bonded (Nakamoto et al., 1970).

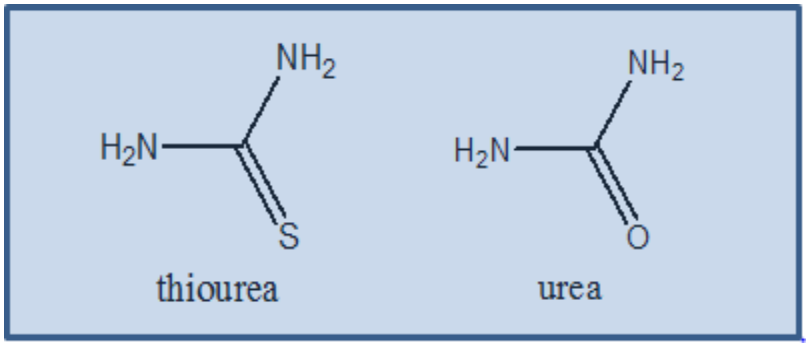

Figure 2.1: Chemical structures of thiourea and urea.

Thiourea having a considerably wide range of applications is a functional organic compound similar to urea, except that the oxygen atom is replaced by a sulfur atom in thiourea **(Figure 2.1)**. The properties of these two ligands differ significantly because of the difference in the electronegativities of sulfur and oxygen atoms. Infrared absorption studies have shown that urea forms nitrogen to metal bond with Pt(II) and Pd(II), but it forms oxygen to metal bonds with Cr(III), Fe(III), Zn(II), and Cu(II) chlorides, whereas in thiourea complexes all the metals are sulphur bonded, except with Ti(IV) which is nitrogen bonded (Srinivasan et al., 2014). The

structure of thiourea complexes has been studied by X-ray diffraction analysis. In $(Ni(tu)_4Cl_2)$ complex, (tu= thiourea), the nickel atom is surrounded by four sulfur atoms at 2.45 Å and two chlorine are at 2.40 Å in the trans-octahedral sites (Alfurayj., 2015). Lopez-Castro and Trater also determined the structure of high spin compounds and concluded that in diamagnetic Ni (II) complex, the Ni-S distance is between 2.1 and 2.3 Å, whereas in the six-coordinated complex it is between 2.4 and 2.6 Å. Lopez and Trater findings are in accordance with the ligand-field theory which predicts that the stronger field produced by the ligand closer to nickel metal will cause the dy electrons to pair in the dz^2 orbitals and produce a diamagnetic complex with no close neighbors in the z direction. For the unidentate ligands like thiourea and urea, the coordination ability will depend not only on the electronegativity but also on the total dipole moment (μ) of the ligand which can be calculated using the formula.

$$\mu=P+\alpha E \qquad \textbf{(Equation 2.1)}$$

Where P is the permanent dipole moment, α is the polarizability and E is the inducing electrostatic field. Thiourea and urea are uncharged ligands (L) and on an electrostatic model the induced dipole of L will be oriented towards M^+ to form a complex:

$$\Delta H= \frac{Z_e(P+P^2)}{r_1^2} \qquad \textbf{(Equation 2.2)}$$

Here ΔH is a bond strength, Z_e is an effective nuclear charge on center metal, r_1^2 is the distance between the center of M^+ and center of the dipole. The large value of r_1 and the smaller value of P for sulfur when compared to oxygen probably outweigh the effect of the large value of P^2 and would expect $R_2O>R_2S$ on the covalent model. Person classified metal ions and ligands as "hard "and "soft" Lewis acids and bases. He suggested a general rule that hard acids bond

strongly to hard bases and soft acids bond strongly to soft bases. Person's hard and soft acids correspond roughly to class (a) and (b) metals respectively. Class (a) metals are those which form the most stable complex with the first ligand atoms of each group and class (b) are classified as those which form the most stable complexes with the second or subsequent ligand atoms. Class (a) metals O>S>Se>Te, for class (b) S>O.

This study also reports on the binding competition between the ligands containing chalcogenides atoms of sulfur (thiourea) and oxygen (urea) to the metal ion of cadmium (II) and nickel (II). The ability of binding of these atoms to the center metal gives the advantage of these compounds to be used as single precursors in the preparation of semiconducting metal chalcogenides nanoparticles. The different mode of binding of these chalcogenides atoms can have a significant effect on the morphological properties of the nanoparticles that can be synthesized from these complexes. The synthesis of nanoparticles will also be part of this work, the synthesized metal complexes of thiourea and urea will be used here to synthesize metal chalcogenides nanoparticles.

2.1.2 Metal chalcogenides complexes

There has been an interest in the study of new non-linear optical crystals made from thiourea, urea and metal. Rao and Kalainathan in 2012 reported on the growth and characterization of the new non-linear optical crystal of thiourea-urea zinc by slow evaporation technique at room temperature. The synthesis of new non-linear optical crystals of thiourea-urea zinc complex using simple method involving urea and thiourea ligands at room temperature. This method can be a breakthrough in the synthesis of dichalcogenide metal complexes. Most of bidentate metal dichalcogenides are not easy to synthesize at room temperature and are also expensive

to synthesize. The growth of thiourea-urea zinc crystals was done by Srinivasan and co-workers. It was found that the synthesized complex was zinc thiourea crystals and not the previously reported thiourea-urea zinc **(Figure 2.2)**. With their findings and the lack of supporting information from the first work on the synthesis of the new non-linear complex of thiourea urea zinc, they out ruled the conclusion made by Madhurambal on the synthesis of this new complex and from their work conclude that the synthesized complex is well-known zinc thiourea crystals.

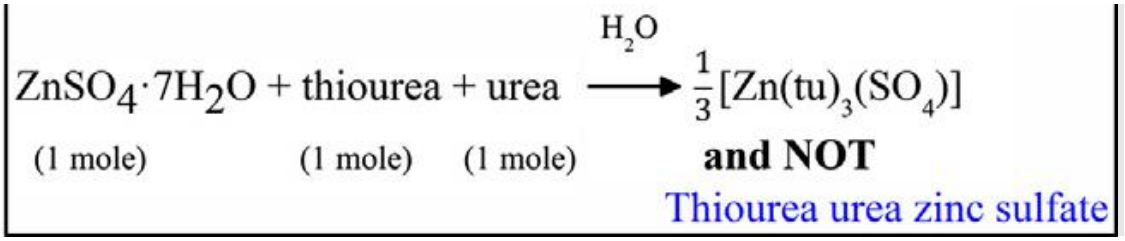

Figure 2.2: Reaction equation of Zinc sulfate with thiourea and urea.

This study also investigated the synthesis of semi-organic nonlinear optical thiourea-urea metal using cadmium and nickel metals. The synthesized complexes were further used as single source precursors for the synthesis of cadmium and nickel chalcogenides nanocrystals. The type of chalcogenide in these complexes can also affect the ability of the compound to undergo certain reactions, and this gives this type of complexes the potential to be used as the single precursor for the synthesis of semiconductor metal chalcogenide nanoparticles. Recently different researchers are exploring the effect of the chalcogenides complexes on the synthesized of semiconducting nanoparticles synthesized.

Chapter 3

Synthesis and characterization of metal chalcogenides, and dichalcogenides complexes

3.1 Chemical reagents

Cadmium (II) chloride, nickel (II) chloride, thiourea, and urea were purchased from Sigma Aldrich and used as purchased. Acetone, ethanol, and methanol were also purchased from Sigma Aldrich and used without any purification (analytical grade).

3.2 Instrumentation

3.2.1 FT-IR Spectroscopy

Infrared spectra were recorded on a FT-IR Perkin Elmer 400 spectrometer. Spectra were measured over the range of 400 to 4000 cm^{-1} to determine the complexes functional groups.

3.2.2 CHNS Elemental analysis

Elemental analysis for the purity of complexes was performed on a CARLO ERBA elemental analyzer for determination of C, H, N, and S.

3.2.3 Thermogravimetric analysis

Thermogravimetry analysis (TGA) was performed from 30 ºC up to 900 ºC on Perkin Elmer Pyris TGA with nitrogen flow and a heating rate of 10-20 ºC/min, to determine the thermal stability of the complexes.

3.3 Preparation of the complexes

Cadmium thiourea, cadmium urea, complexes and nickel thiourea, nickel urea, complexes were prepared as outlined below. The complexes were prepared by refluxing the mixture of materials of interest in ethanol to give white and yellowish powders and clear crystals by slow evaporation at room temperature after refluxing.

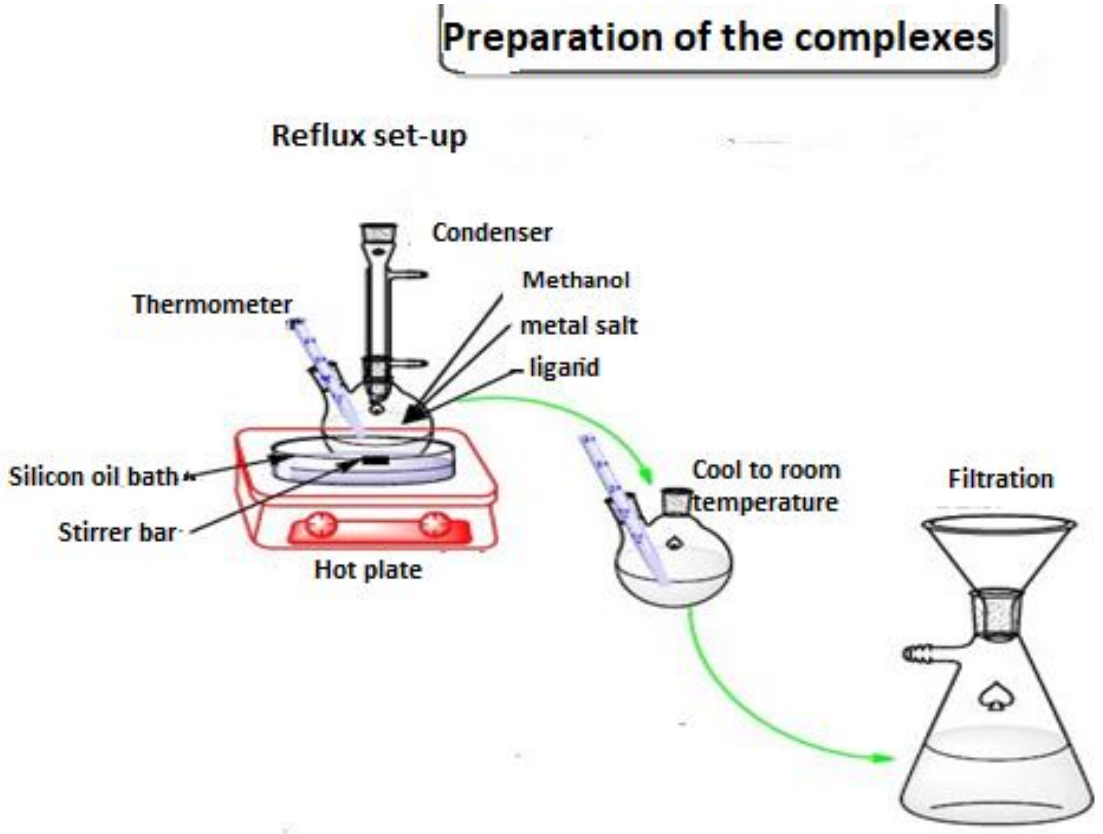

Figure 3.1: Diagram for the synthesis of complexes.

The synthesis of complexes was done using the simple reaction of metal salt (cadmium and nickel) with ligands (thiourea and urea) as represented on the following reaction equations

Reaction

- ✓ $CdCl_2/NiCl_2 + SC(NH_2)_2 \rightarrow$ cadmium/nickel thiourea
- ✓ $CdCl_2/NiCl_2 + CO(NH_2)_2 \rightarrow$ cadmium/nickel urea
- ✓ $CdCl_2/NiCl_2 + CO(NH_2)_2 + SC(NH_2)_2 \rightarrow$ cadmium/nickel thiourea

3.3.1 Synthesis of cadmium chalcogenides complexes

(a) Bis (thiourea)cadmium chloride

$CdCl_2.6H_2O$ (2.28 g; 10 mmol) was dissolved in 20 ml ethanol and 0.76g of thiourea was added. The mixture was refluxed for hour with heating at 40 ºC and a white solution resulted

as the end product. The white solution was filtered to remove any traces of unreacted materials and left in an open beaker over a night at room temperature to crystallize by slow evaporation. The following day the crystals were obtained, filtered, washed twice with ethanol and dried in open air

Chemical reaction: $CdCl_2.6H_2O + 2[CS(NH_2)_2] \longrightarrow Cd[CS(NH_2)_2]_2Cl_2 + 6H_20$

(b) Bis (urea) cadmium chloride

$CdCl_2.6H_2O$ (2.28 g; 10 mmol) was dissolved in 20 ml ethanol and 0.60g of urea was added. The mixture was refluxed for 1 hour with heating at 40 ºC and a white solution resulted in the end as the product. The white solution was filtered to remove any traces of unreacted materials and left in an open beaker at room temperature to crystallize by slow evaporation. The following day the white powder was obtained, filtered, washed twice with ethanol and dried in open air.

Chemical reaction: $CdCl_2.6H_2O + 2[CO(NH_2)_2] \longrightarrow Cd[CO(NH_2)_2]_2Cl_2 + 6H_20$

(c) Bis (thiourea) cadmium chloride*

$CdCl_2.6H_2O$ (2.28 g; 10 mmol) was dissolved in 20 ml ethanol and 0.76g of thiourea and 0.60g of urea was added simultaneously. The mixture was refluxed for 1 hour with heating at 40 ºC and a white solution resulted in the end as a product. The white precipitate was filtered to remove traces of unreacted materials and left in an open beaker at room temperature to crystallize by slow evaporation. The following day a white powder was obtained, filtered, washed twice with ethanol and dried in open air. Chemical reaction:

$CdCl_2.6H_2O + 2[CO(NH_2)_2] + 2[CS(NH_2)_2] \longrightarrow Cd[CS(NH_2)_2]_2Cl_2 + 6H_20 + 2[CO(NH_2)_2]$

3.3.2 Synthesis of nickel chalcogenides complexes

(a) Nickel thiourea

$NiCl_2.6H_2O$ (2.38 g; 10 mmol) was dissolved in 20 ml ethanol and 0.76g of thiourea was added. A yellowish-green solution was obtained and refluxed for 1 hour with heating at 40 ºC. The yellow solution was filtered to remove any traces of unreacted materials and left in an open beaker at room temperature to crystallize by slow evaporation over a night. The following day the yellow powder obtained was filtered, washed twice with ethanol and dried in open air.

Chemical reaction $NiCl_2.6H_2O + 2[CS(NH_2)_2] \rightarrow Ni[CS(NH_2)_2]_2Cl_2 + 6H_2O$

(b) Nickel urea

$NiCl_2.6H_2O$ (2.38 g; 10 mmol) was dissolved in 20 ml ethanol and 0.60g of urea was added. The green solution formed was refluxed for 1 hour on heating at 40 ºC and filtered to remove traces of unreacted materials. The solution was left in an open beaker at room temperature to crystallize by slow evaporation. The following day the green powder obtained was filtered, washed twice with ethanol and dried in open air.

Chemical reaction $NiCl_2.6H_2O + 2[CO(NH_2)_2] \rightarrow Ni[CO(NH_2)_2]_2Cl_2 + 6H_2O$

(c) Nickel thiourea*

$NiCl_2.6H_2O$ (2.38 g; 10 mmol) was dissolved in 20 ml ethanol, 0.76 g of thiourea and 0.60g of urea was added. The mixture was refluxed for 1 hour with heating at 40 ºC and a yellowish-green solution was formed. The solution was filtered to remove any traces of unreacted materials and left in an open beaker at room temperature to crystallize by slow evaporation. The following day the yellow crystals obtained was filtered, washed twice with ethanol and dried in open air.

Chemical reaction $NiCl_2.6H_2O + 2[CS(NH_2)_2] + 2[CO(NH_2)_2] \rightarrow Ni[CS(NH_2)_2]_2Cl_2 + 6H_2O$

Table 3.1: List of all complexes synthesized in Section 3.3

Section	Reaction (Solvent: Ethanol)	Mole ratio	Synthesized Complex
3.3.1 (a)	Cadmium chloride + thiourea	1:1	Bis (thiourea) cadmium chloride
(b)	Cadmium chloride + urea	1:1	Bis (urea) cadmium chloride
(c)	Cadmium chloride + thiourea + urea	1:1:1	Bis (thiourea) cadmium chloride*
3.3.2 (a)	Nickel chloride + thiourea	1:1	Nickel thiourea
(b)	Nickel chloride + urea	1:1	Nickel urea
(c)	Nickel chloride + thiourea + urea	1:1:1	Nickel thiourea*

3.4 Results and Discussion

Complexes synthesized in this work were stable and were prepared by refluxing metal salt and ligand at the room temperature. They are also environmentally friendly and low cost, the interest in the thiourea and urea ligands is their ability to easily donate or provide sulfur and oxygen ion to the heavy metals such as Cadmium or Nickel. Thiourea and urea are also easy ligands to work with for the formation of metal chalcogenide complexes, like cadmium thiourea because here thiourea already have high affinity for cadmium metal. The complexes were characterized using Fourier transform infrared (FT-IR) spectroscopy, Elemental analysis (EL) and thermal gravimetric analysis (TGA) and further used as single source precursors for the synthesis of metal chalcogenide nanoparticles.

3.4.1 FTIR spectral analysis of thiourea, urea, and their cadmium chalcogenides and dichalcogenide complexes

Infrared spectroscopy is a relevant technique in determining the binding mode of the ligand to the metal centre. More studies on infrared absorption spectra were reported for some metal thiourea and urea complexes (Srinivasan *et al*., 2014). Thiourea, urea and their derivatives are

well known to have the ability of binding to metal atoms through sulfur (thiourea) and oxygen (urea) atom. However in some instances, this ligand bond to the metal atom through a nitrogen atom, hence it is important to confirm the bonding of this ligands to metals using techniques like FTIR. The figures below show infrared spectra of the thiourea, urea and their synthesized metal complexes for the determination of their binding mode.

(a) Thiourea and its cadmium complex

Figure 3.2 shows the infrared spectra of thiourea ligand (a) and cadmium thiourea complex (b). The stretching mode between 1200 to 1117cm^{-1}, for both thiourea and its cadmium complex are due to C-N or N-C-N stretching frequencies are not disturbed. The band observed between the ranges (3395 to 3100 cm^{-1}) on free ligand is assigned to the N-H stretching and there was no significant change in the frequency of this N-H stretching band on the formation of cadmium thiourea complex. This indicates that the nitrogen to metal bonds are not present and therefore the bonding was through the sulphur atom due to the change in the thiourea C=S (from 730 cm^{-1} for thiourea to 715 cm^{-1} for cadmium thiourea), this change to lower frequency during the formation of the complex, confirm the metal to sulphur atom bond. This spectrum shows that the cadmium thiourea complex was successfully synthesized by reaction of cadmium chloride with thiourea at a minimal temperature.

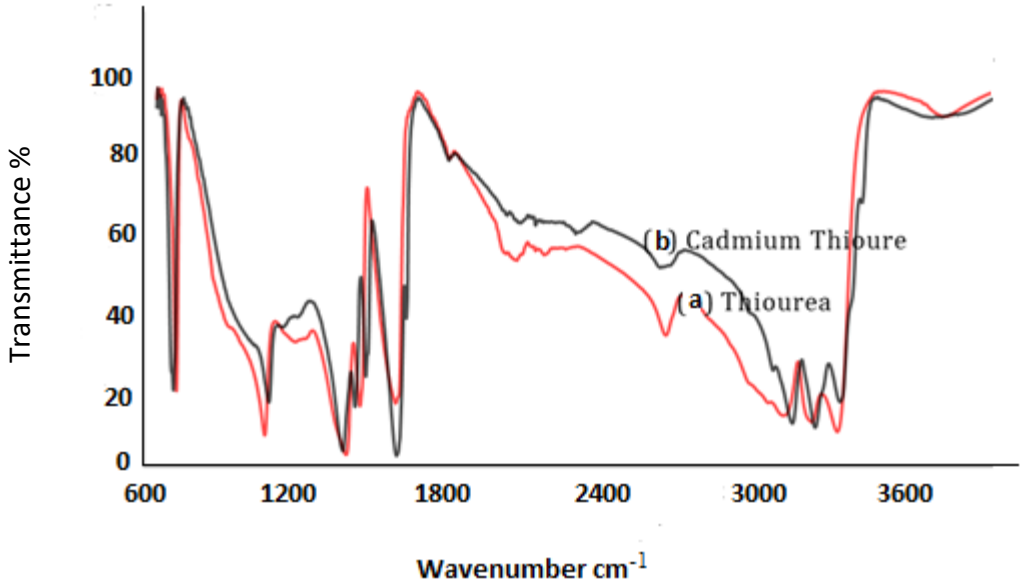

Figure 3.2: Infrared spectra of thiourea (a) and its cadmium complex (b)

(b) Urea and its cadmium complex

Urea molecule mostly coordinates with metal ions such as cadmium as a monodentate ligand through the oxygen atom, forming a C=O·····M bond (M is the metal).The urea ligand, like thiourea ligand, also has the potential of binding through the nitrogen atoms. The mode of coordination of urea with the metal ions seems to be dependent upon the type and nature of the metal ion. To know whether urea is coordinated through oxygen or nitrogen atom, the shift in C=O or N-H vibrational spectrum will give information to how the urea is coordinated to the metal ion. **Figure 3.3** shows the infrared spectra of urea (a) and its cadmium complex (b). The observed stretching frequency for N-H at the range 3437 to 3267 cm^{-1} shifted to a slightly higher frequency on the formation of the complex, indicating no nitrogen to metal bond present. The presence of a carbonyl vibration (C=O) at 1677 cm^{-1} for the free urea ligand, shifted to 1600 cm^{-1} in the spectra of the complex, indicating that a coordinate bond is formed between oxygen and the central metal atom.

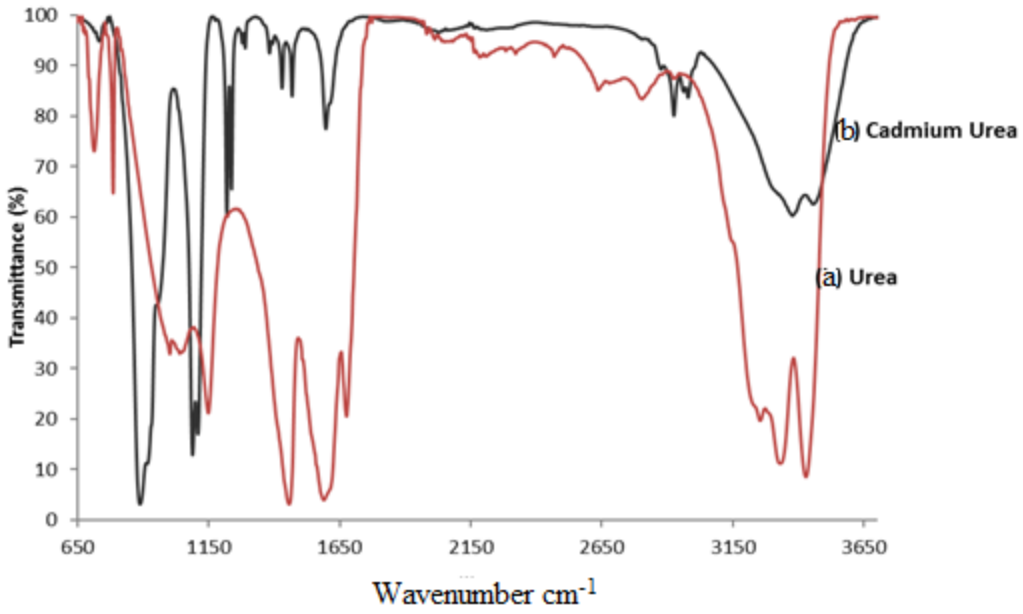

Figure 3.3: Infrared spectra of urea (a) and its cadmium complex (b)

(c) Cadmium urea, cadmium thiourea* and cadmium thiourea complexes.

Figure 3.4 show the infrared spectrum of the cadmium thiourea, cadmium urea and cadmium thiourea*. The cadmium thiourea* spectrum was compared to the spectra of cadmium thiourea on **Figure 3.2** and cadmium urea on **Figure 3.3** to confirm if the synthesized cadmium thiourea* complex is indeed cadmium thiourea, or the new complex of thiourea-urea cadmium. The FTIR spectrum of this complex indicates that the prepared complex is the well-known cadmium thiourea, not the ideal complex of thiourea-urea cadmium complex or either cadmium urea. This complex will be named cadmium thiourea* through-out this work to differentiate it from the cadmium thiourea from cadmium chloride and thiourea reaction. It can be observed for both spectral of cadmium thiourea and cadmium thiourea* in **Figure 3.4** that they follow the same trend or properties.

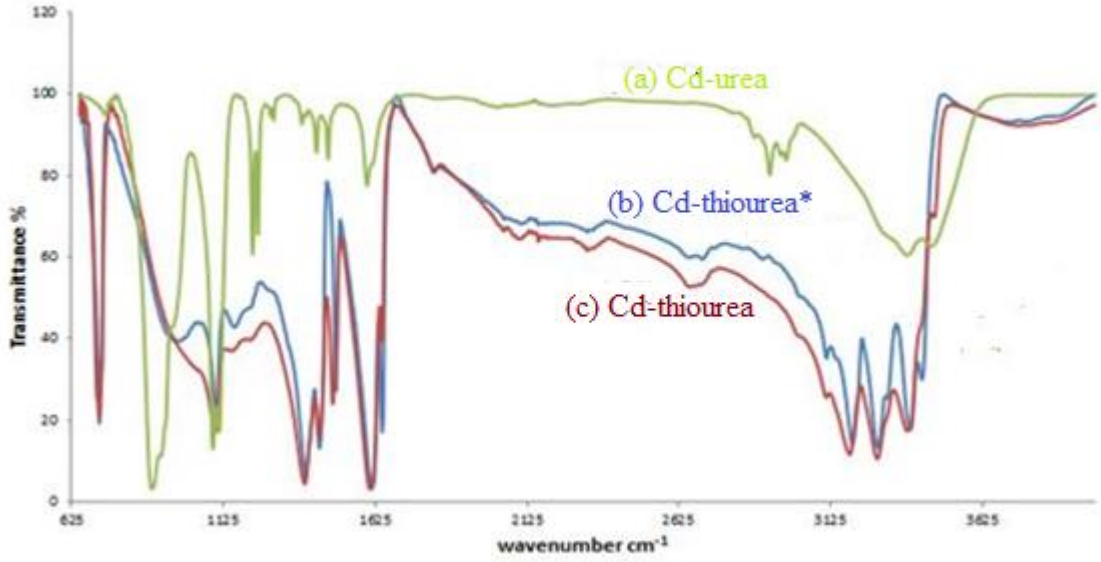

Figure 3.4: FTIR spectra of cadmium thiourea, cadmium urea, and cadmium thiourea*

The strong peak at the wavelength 715 cm^{-1} for both complexes of cadmium thiourea and complex 1, which is not present on cadmium urea complex, is assigned to the C=S stretching band. From this observation, we can conclude that the reaction of cadmium chloride with urea and thiourea crystals, with the mole ratio of 1:1:1 lead to the formation of cadmium thiourea* complex, not the expected thiourea-urea cadmium. The percentage yield of the formed complex for the reaction of thiourea, urea, and cadmium chloride is less than 50%, this can be due to the unreacted urea crystals that were washed away during the washing process of the synthesized cadmium thiourea* complex, leaving only the crystals of cadmium thiourea*. This can be explained by the coordination chemistry of cadmium and chalcogenides ligand field theory which state that the soft acid cadmium atoms have a high affinity for soft base sulfur atom, rather than the hard-base oxygen, hence the above reaction results in cadmium thiourea*. Also there are no traces of cadmium urea in the complex according to the FITR spectrum of synthesized complex.

3.4.2 FTIR spectral analysis of thiourea, urea and their nickel chalcogenide and dichalcogenide complexes

In another set of experiments, the cadmium metal was replaced with nickel metal to synthesize nickel thiourea, nickel urea and nickel thiourea*. Where by nickel thiourea* was synthesized by the reaction of nickel chloride with thiourea and urea crystals.

(a) FTIR spectra of urea and nickel urea complex

Figure 3.5 shows that the nickel urea complex was successfully synthesized from nickel chloride and urea ligand. The N-H stretching frequency represented by the peak around 3500 wavenumbers was shifted to high frequency during the formation of the complex.

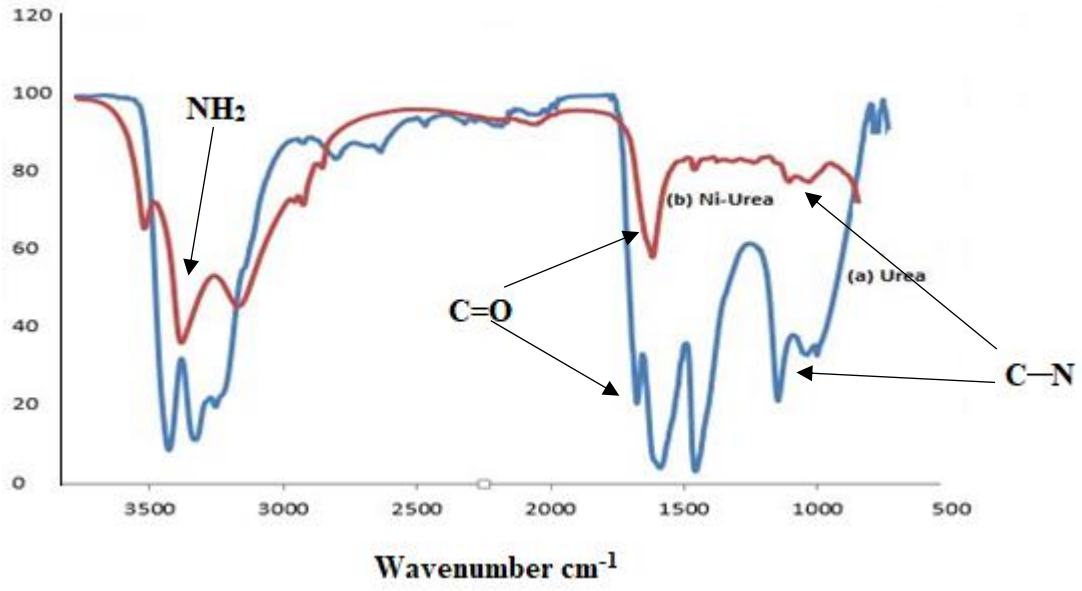

Figure 3.5: FTIR spectra of urea (a) and its nickel complex (b).

The stretching frequencies around 3500 cm^{-1} for both urea and nickel urea are for the amides group in urea ligand, no shift or change in this stretching frequency indicates that the nickel metal did not bond through nitrogen atom with the urea ligand. The stretching frequency at 1700 cm^{-1} for urea and 1600 cm^{-1} for nickel urea is for the C=O group, and this stretching frequency shifted from 1700 cm^{-1} to a lower frequency of 1600cm^{-1} on the formation of nickel

urea, this change present that the nickel metal is bonded to the urea ligand through the oxygen atom, which is always the case in most of the work reported on urea ligand complexes with semiconducting metals (Keuleers *et al*., 2000). Other peaks that can be observed from the spectrum can be assigned for C-N modes.

(b) FTIR spectra of thiourea and nickel thiourea complex

The $S{=}CN_2$ modes for thiourea ligand and nickel thiourea complexes observed at around 1500 and 1000 cm^{-1}. **Figure 3.6** show no change in the frequencies respectively on the coordination of urea with the metal. The N-H bands were also not shifted to the lower frequency during the formation of the complex, which indicates that the nitrogen to metal bond is not present.

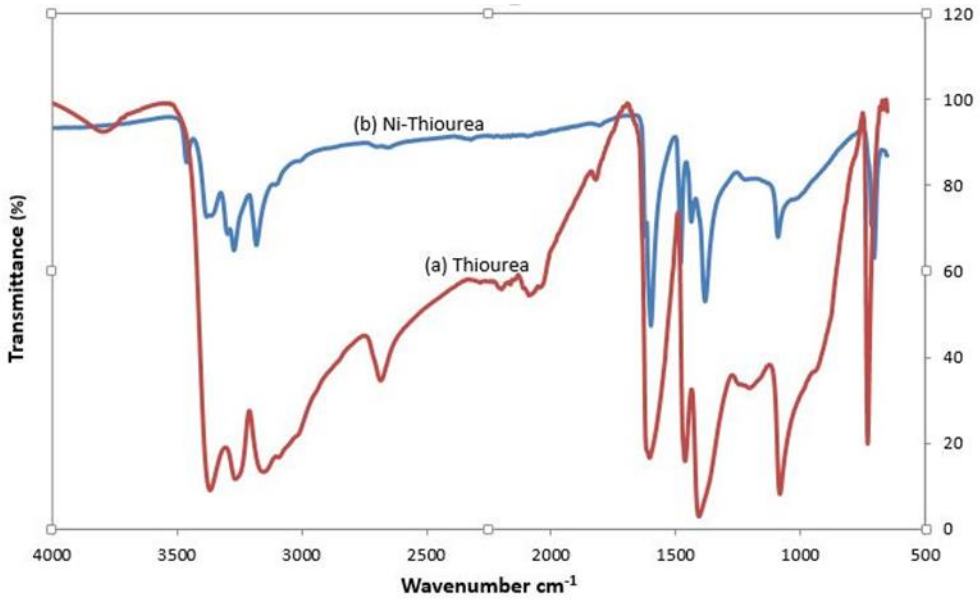

Figure 3.6: FTIR spectra of thiourea ligand (a) and its nickel complex (b).

This information indicates that the only possibility of the metal bonding to thiourea is through a sulfur atom. The free ligand shows a band at 732 cm^{-1}, which is due to C=S stretching and this band shifted to a lower frequency of 711 cm^{-1} on the formation of nickel thiourea complex.

This significant change in C=O band indicates the formation of nickel complex, through the sulfur to metal bond.

(c) FTIR spectra of nickel thiourea, Nickel thiourea* complexes

The below FTIR spectrum in **Figure 3.7** shows the spectrum for nickel thiourea compared with nickel thiourea* with the variation of the urea mole ratio. All complexes as it can be observed from Figure 2.7 resemble the same properties as that of nickel thiourea.

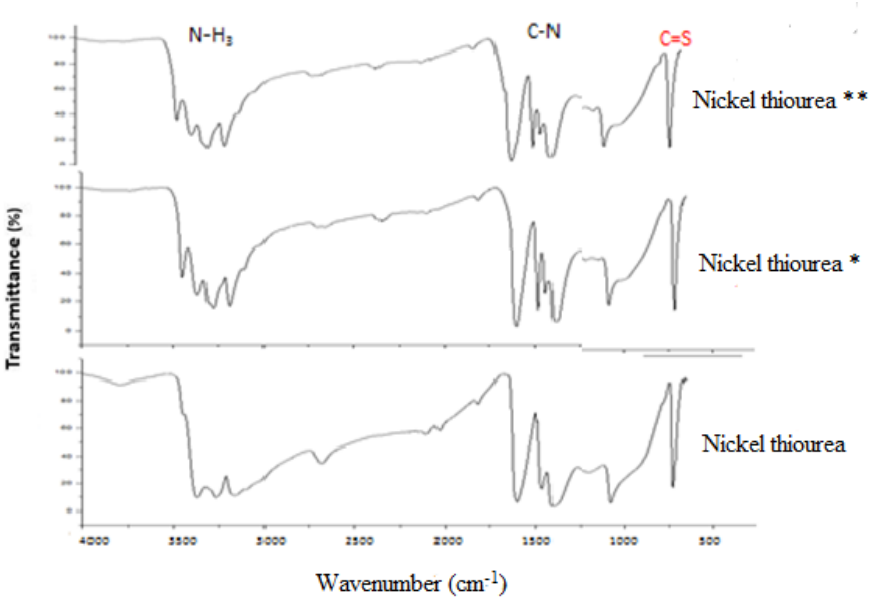

Figure 3.7: FTIR spectra of nickel thiourea and nickel thiourea*.

The mole ratio of urea was increased from 1 mole to 2 and further to 3 moles to increase the amount of the urea in the reaction mixture. It can be observed from the spectra of both complex nickel thiourea* that there complex are similar to nickel thiourea which indicates that the synthesized complexes are nickel thiourea not the expected complex of thiourea-urea nickel. This suggest that nickel also has a strong affinity for a sulfur atom rather than the oxygen atom. There is no evidence from the spectra of the existence of Ni-O(urea) bond in the reaction mixture which indicates that the urea in this reaction mixture did not bond to central nickel

metal, hence both spectral shows the formation of well-known nickel thiourea complex. With the above-mentioned information, the synthesized complexes are nickel thiourea complexes not the thiourea-urea nickel complexes. This contradicts the observation made by Rao and Kalainathan previously reported their work of spectroscopic investigation, nucleation, growth, optical, thermal and second harmonic studies of novel semi-organic nonlinear optical crystal–thiourea urea zinc sulfate (Rao and Kalainathan, 2012).

3.4.3 Thermogravimetric analysis for complexes

The thermogravimetric (TGA) of the complexes were measured under a flow of nitrogen to study the thermal behavior of the synthesized complexes. By heating, the chemical decomposition of the complexes could be studied. Metal compound of thiourea and urea represent an extensive series of sulfur and oxygen bonded complexes with well-established structures. Thermal decomposition studies of this complexes have been studied before and their thermal decomposition led to the formation of the metal sulfide and metal oxide in the main degradation step between 200 °C and 300 °C (Jona, 1966). The thermogravimetric analyses (TGA) were conducted to evaluate the physical behavior of cadmium and nickel chalcogenides of substituted thiourea, urea.

(a) Thermal analysis of cadmium urea and cadmium thiourea complexes

TGA profile for cadmium urea and cadmium thiourea complexes are shown in **Figure 3.8**. The TGA profile for cadmium thiourea indicates that the loss of weight started at around 200 °C, which is due to the loss of chloride. The decomposition continued at 350 °C, with slow evaporation showing the loss of organic part of the molecule, led to the formation of cadmium sulphide which was completed at about 90 °C.

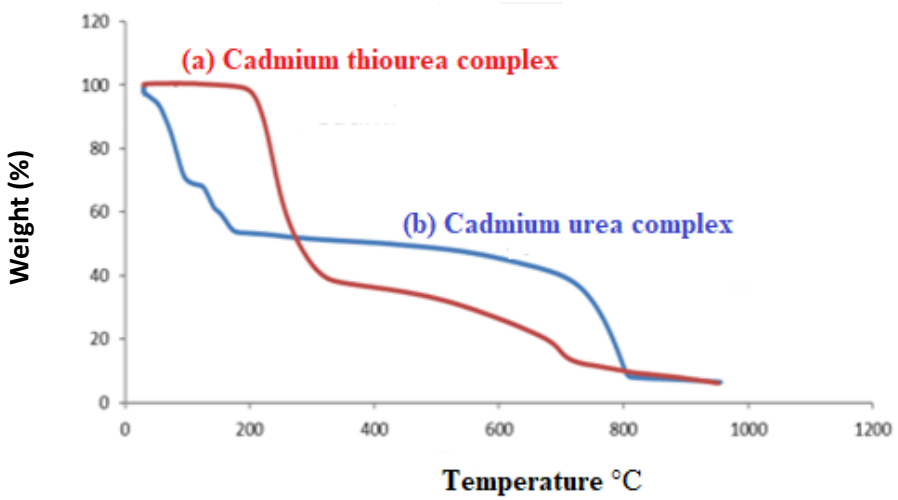

Figure 3.8: TGA profile of (a) cadmium thiourea and (b) cadmium urea.

The TGA profile for cadmium urea complex in **Figure 3.8 (b)** display the initial weight loss at a lower temperature of 80 °C. This was due to the loss of solvent (not well-dried sample) or water-related molecules. The weight loss continued at 100 °C, due to the loss of water traces in the sample and loss of chloride at 200 °C. The decomposition of the sample stabilized at 200-800 °C. The last weight loss at about 800 °C, was due to the loss of other organic molecules leading to the formation of cadmium oxide.

(b) Thermal analysis of nickel urea and nickel thiourea complexes

Figure 3.9 shows the TGA profile of nickel thiourea and nickel urea complexes. Both complexes showed the first decomposition at 200 °C. The first decomposition step is the loss organic part of the complex. The second decomposition at 600 °C for nickel thiourea and 550 °C for nickel urea is associated with the loss of chloride. The complexes stabilize around 800 °C with 15g residual for both complexes.

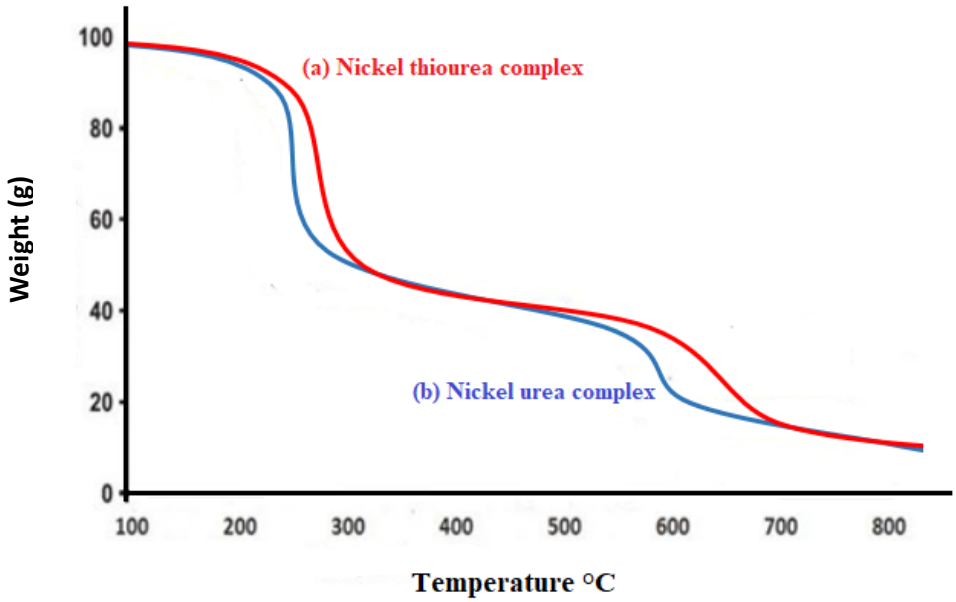

Figure 3.9: TGA profile of (a) nickel urea and (b) nickel thiourea

(c) Thermal analysis of nickel thiourea*

Figure 3.10 shows the TGA profile of nickel thiourea* from reaction of nickel chloride with thiourea and urea, with variation of mole ratio of urea **Figure 3.10 (a)** 1 mole and **Figure 3.10 (b)** 2 moles while keeping both mole ratio of nickel chloride and thiourea at 1 mole. Which exhibited similar decomposition patterns. The complexes show more than two steps of decomposition from 200 °C, which is due to the loss of chloride and organic molecules with decrease in rate of decomposition from 380 °C with slow decomposition till 700 °C where the expectation was the stabilization of the complex weight loss due to the expected residual of nickel sulfide. But in this case complexes continued to decompose till 0g weight which it can be due to instrumental or experimental error.

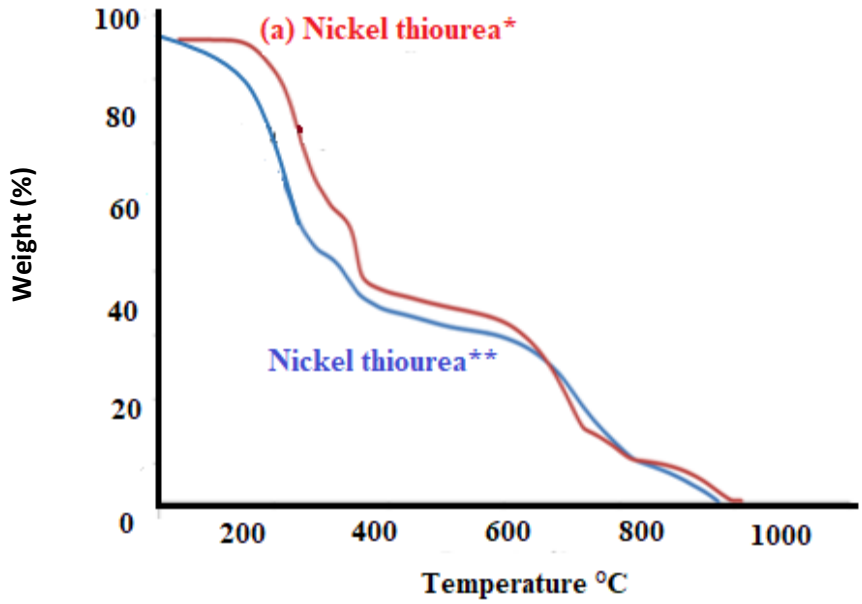

Figure 3.10: TGA profile of (a) nickel thiourea* and (b) nickel thiourea **

The weight loss at 700 °C, can be ascribed to the loss of other organic molecules leading to the formation of metal chalcogenide. The similarity in the decomposition stages of this two complexes suggests that the synthesized complexes are of cadmium thiourea as it was observed from the FTIR spectrum results and elemental analysis.

(d) Thermal analysis of cadmium thiourea***** and cadmium urea******

Figure 3.11 shows the TGA profile of cadium thiourea*, **Figure 3.11 (a)** and cadmium thiourea**, **Figure 3.11 (b)** synthesized from the reaction of cadmium chloride, thiourea and urea with the variation of urea mole ratio. The amount of urea was increased from 1 mole to 3 moles in the synthesis of cadmium thiourea* and cadmium thiourea** while keeping that of cadmium chloride and thiourea at constant (1 mole).

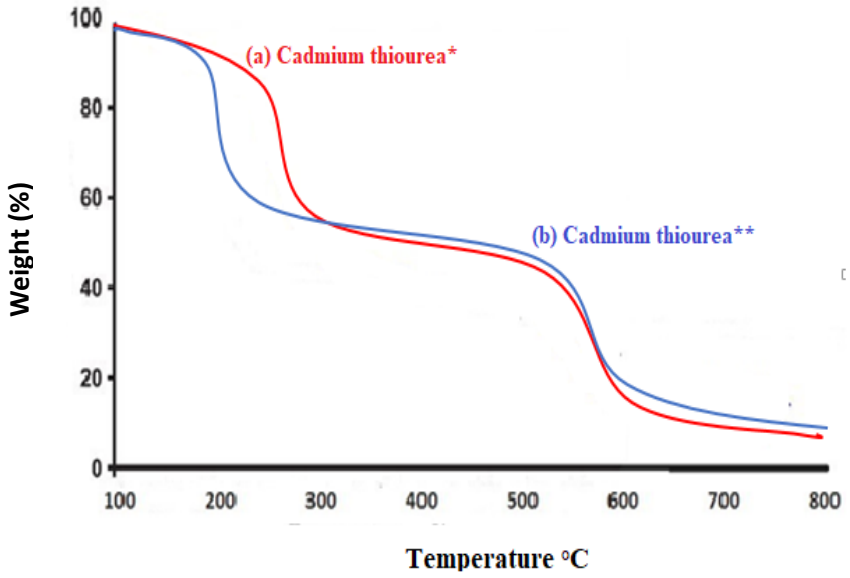

Figure 3.11: TGA profile of cadmium thiourea* (a) and cadmium thiourea** (b)

Both patterns show similar TGA profile with minimal differences. Decomposition started at 200 °C for cadmium thiourea* and 250 °C for cadmium thiourea**, this weight loss is due to the loss of organic molecule from the complex. Weight loss stabilized around 250 °C to 600 for cadmium thiourea* and from 300°C to 600 C for cadmium thiourea**, where the second decomposition stage take place due to the loss of chloride.

The reaction mixture of metal (cadmium or nickel) with urea and thiourea can lead to more than one possibility. The formation of metal thiourea complex or metal urea, or also a new complex of thiourea-urea metal. Theoretical information indicates that metals like cadmium and nickel have higher affinity for sulfur than oxygen hence the previous study done by Thomas and co-wokers on the formation of a new complex of thiourea-urea nickel complex showed that this type of reaction mixture led to the formation of nickel thiourea complex not thiourea-urea nickel ((Thomas *et al.*, 1999). In this study, the same observation on the attempt to synthesize thiourea-urea nickel and thiourea-urea cadmium complexes was observed and here the amount of urea in the reaction system was increased to 3 moles rather 1 mole to give urea

more bonding advantages over thiourea counterpart to form a necessary bond with the center metal.

3.4.4 Summary of results

The above FTIR spectral and TGA results of this study reveal that the formed complexes from the reaction of metal (cadmium or nickel) with thiourea and urea lead to a well-known complexes of nickel thiourea and cadmium thiourea not the expected thiourea-urea nickel nor thiourea-urea cadmium. In both cases were the amount of urea in the reaction system was increased, the resulting complexes were of metal thiourea complex.

Chapter 04

Synthesis and characterization of metal chalcogenide nanoparticles from thiourea and urea-based cadmium and nickel complexes

4.1 Chemical reagents

Cadmium and nickel complexes used here were synthesized and disused in chapter three. Acetone, methanol, hexadecylamine, and tri-n-octylphosphine were purchased from Sigma Aldrich (South Africa) and used as purchased without any further purification.

4.2 Instrumentation

4.2.1 Optical properties

The absorption spectra of the metal chalcogenides were measured using a Perkin Elmer Lambda 20 UV-Vis Spectrophotometer. The samples were placed in quartz cuvettes (1-cm path length) with toluene as the solvent. Emission spectra of the particles were recorded on a Perkin-Elmer LS 45 photoluminescence (PL) spectrometer with a xenon lamp at room temperature. The samples were placed in glass cuvettes (1 cm) with toluene as solvent.

4.2.2 X-ray diffraction analysis

X-ray diffraction (XRD) patterns of powdered samples were carried out on a D8 diffractometer. Samples were placed in a silicon zero background sample holder. Measurements were taken using a glancing angle of incidence detector at an angle of 2°, for 2θ values over 20° – 60° in steps of 0.05° with a scan speed of 0.01 °2θ.$^{s-1}$.

4.2.3 Electron microscopy

TEM images were obtained using Joel JEM-2100 TEM operating at 200 kV. The samples were prepared by placing drops of a dilute solution of the sample in toluene onto a copper grid. The sample was allowed to dry completely at room temperature.

4.3 Synthesis of cadmium and nickel chalcogenide nanoparticles

Hexadecylamine (HDA) was degassed under nitrogen gas and heated to 160 $^{\circ}$C in a three-neck round-bottom flask. The metal (cadmium/nickel) chalcogenide (thiourea/urea) precursors was dispersed in trioctylphosphine (TOP) and injected into the hot solution of HDA. The reaction

was maintained at 160 °C for 1 hour while stirring. The solution was cooled to approximately 70 °C, after which excess acetone was added and the solid was isolated by centrifugation. The solid was further washed several times with acetone and left to dry at room temperature.

Table 4.1: Complexes and parameters used for synthesis of cadmium and nickel chalcogenide nanoparticles

Complexes	Temperature	Surfactant	Time	End Product
$CdCl_2(CS(NH_2)_2)_2$	160	HDA	1 hour	CdS
$CdCl_2(CO(NH_2)_2)_2$	160	HDA	1 hour	CdO
$CdCl_2(CS(NH_2)_2)_2$*	160	HDA	1 hour	CdS
$NiCl_2(CS(NH_2)_2)_2$	160	HDA	1 hour	NiS
$NiCl_2(CO(NH_2)_2)_2$	160	HDA	1 hour	NiO
$NiCl_2(CS(NH_2)_2)_2$*	160	HDA	1 hour	NiS

4.4 Results and Discussion

4.4.1 CdS and CdO nanoparticles from Cd-thiourea, complex 1 and Cd-urea

(a) Qualitative analysis and optical properties of CdS nanoparticles

The changes in the morphological properties of the nanoparticles affect the optical properties, small particle size exhibit a high optical absorption due to the existence of discrete energy levels of the electron. One of the major factors that influence the growth of the particles is temperature. The temperature of the reaction influences the particle size with higher temperatures favoring larger particles size. The reaction temperature also affects the shape of the nanoparticles due to the competition between the kinetic and thermodynamic growth regime. Other factors that play an important role in determining the morphological properties of nanoparticles include precursor concentration, surfactant, and stirring rate (Ramasamy *et al.,* 2010). These conditions need to be optimized during synthesis reaction of the nanoparticles.

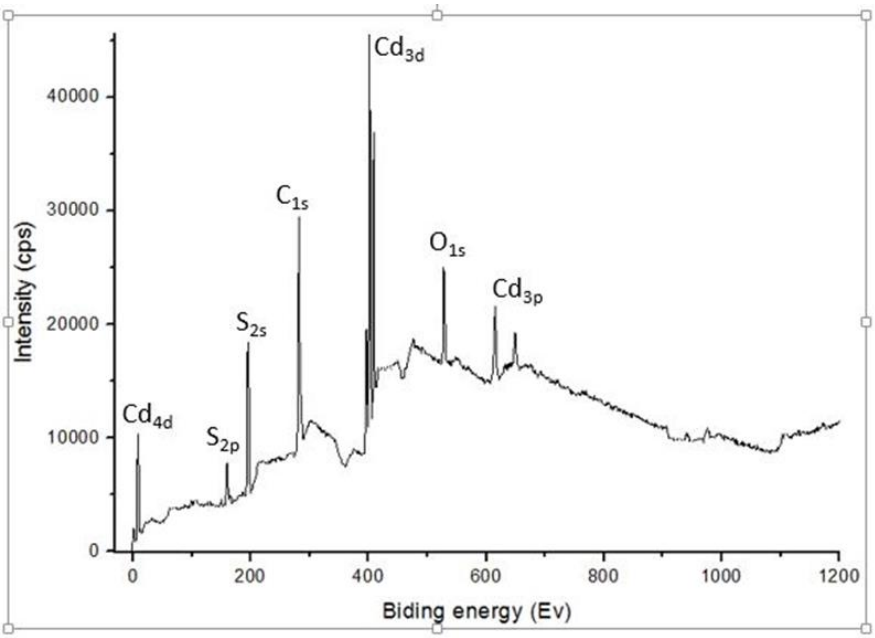

Figure 4.1: X-ray photoelectron spectrum of CdS nanoparticles from cadmium thiourea*.

Figure 4.1 depict the XPS spectrum of the CdS particles from cadmium thiourea with all the binding energies calibrated using C 1s (284 eV). The spectrum provides information on the existence of Cd, S and O elements in the sample. The peaks of C and O can be related to reference and absorbed gaseous molecules on the exposure of the sample to atmospheric air. The binding energies of Cd $3d_{5/2}$ and Cd $3d_{3/2}$ are identified around 400 eV, respectively, with double peaks at that region of the spectrum. The two peak at around 200 eV is probably due to S 2p and S 2s transitions. This XPS survey spectrum corresponds with XPS data reported by others (Rengaraj *et al*., 2011; Huang *et al*., 2012). From the XPS survey spectrum above, we can see that the nanoparticles from complex 1 are of cadmium sulfide.

It is well-known that group II–IV semiconductor nanoparticles exhibit a huge change in their optical absorptions when their size reduces to less than 100 nanometers, and also the change in the shape of nanoparticles affect their optical absorption position on the spectrum**.** This makes the optical characterization of the nanoparticles significant tool for characterization of nanoparticles**. Figure 4.2** shows the absorption spectra of CdS nanoparticles, the emission spectra are shown in **Figure 4.3**. The Absorption spectrum on **Figure 4.2 (a)**, shows CdS nanoparticles synthesized from cadmium thiourea and spectrum on **Figure 4.2 (b)** is CdS nanoparticles from complex 1, and emission spectrum **Figure 4.3 (a)** shows CdS nanoparticles from cadmium thiourea and spectrum on **Figure 4.3 (b)** is CdS nanoparticles from complex 1. The CdS materials were synthesized under the same reaction parameters which are temperature, concentration, capping agent, reaction time, and stirring rate. These reaction conditions play an important role in determining the morphological properties of nanoparticles.

HDA was used in all experiments as the capping agent, TOP was used as a solvent and reaction time of 60 minutes with 160 °C reaction temperature. Bulk crystallites of CdS usually show absorption band edge at 515 nm (2.41 eV). The absorption spectra shown on **Figure 4.2** are both blue shifted from the bulk CdS band edge of 515 nm. The blue shift observed in the spectra can be related to the formation of the CdS nanomaterials from the bulk CdS material when the size and shape change from bulk to nano-size, thus the observation of the shifts in the spectra. The CdS nanomaterial from cadmium thiourea precursor shown on **Figure 4.2 (a)** have a band edge at 475 nm (2.61 eV), and the CdS nanomaterial from cadmium thiourea* shown on **Figure 4.2 (b)** have band edge at 460 nm (2.70 eV), which is slightly high in energy than that of CdS nanoparticles on **Figure 4.2 (a)**. This difference in the band edges of CdS nanomaterials is due to the difference in size and shape of the synthesized nanomaterials. This shows that the different sources of precursors can affect the morphology of the synthesized nanomaterials. The analyses of cadmium thiourea and cadmium thiourea* in chapter 03 showed little difference in the nature of this complxes. Thus the cadmium sulfide nanoparticles from this two complexes exhibit slight differences in optical properties. From this, it can be concluded that the reaction of cadmium chloride, thiourea and urea reaction produce cadmium thiourea, not thiourea-urea cadmium complex nor cadmium thiourea and the optical properties of the nanoparticles synthesized from this complex exhibit that of CdS nanoparticles.

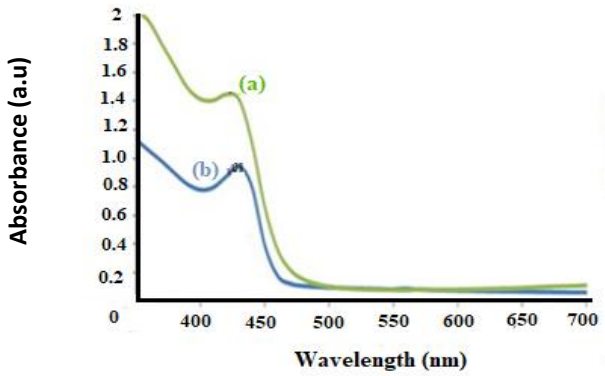

Figure 4.2: CdS absorption spectrum (a) from cadmium thiourea and spectrum (b) from cadmium thiourea*

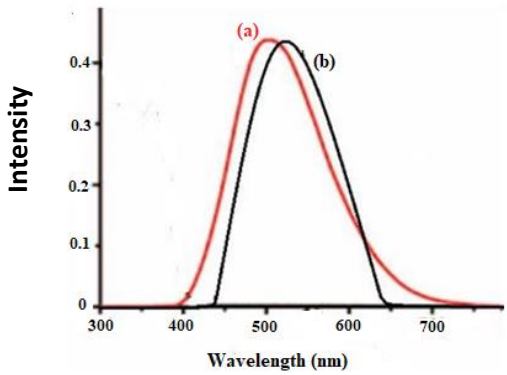

Figure 4.3: CdS emission spectrum (a) from cadmium thiourea and spectrum (b) from cadmium thiourea*

The photoluminescence of the CdS nanomaterials from cadmium thiourea complex is shown on **Figure 4.3 (a)** and shows the maximum emission peak of 500 nm which is red-shifted from the maximum absorption peak (420 nm) with the stoke shift of 80 nm. The emission spectrum of CdS nanomaterial from cadmium thiourea* is shown on **Figure 4.3 (b)** with the maximum emission peak of 550 nm, also red shifted from the absorption peak with the stoke shift of 120 nm. As the diameter of the nanomaterials increases, the red shift of the maximum emission peak from the absorption peak decreases and disappears beyond a certain radius (Moloto *et al.*, 2009). Larger stoke shift on emission spectrum, present well-passivized nanoparticles with smaller diameter, thus smaller size of the nanoparticles.

(b) Structural properties of CdS nanoparticles

Figure 4.4 and 4.5 are XRD patterns of HDA capped CdS nanoparticles from cadmium thiourea and cadmium thiourea* complex. The previous study of structural characterization of CdS nanoparticles shows that the CdS nanoparticles exist in three phases, which are a cubic, orthorhombic and hexagonal phase. The existence of a mixture of cubic with hexagonal phase with the predominance of one over other was reported by (Joshi, 2004). The orthorhombic phase is a very rare structure in CdS nanoparticles. The XRD pattern on **Figure 4.4** shows the

hexagonal phase nanoparticles (100, 002, and 101 planes), with sharp peaks, other peaks present 102, 112, and 104 planes confirms the structure of hexagonal phase. The peaks that are indentified with * can be assigned to the organic groups that are found in the used capping agent (HDA).

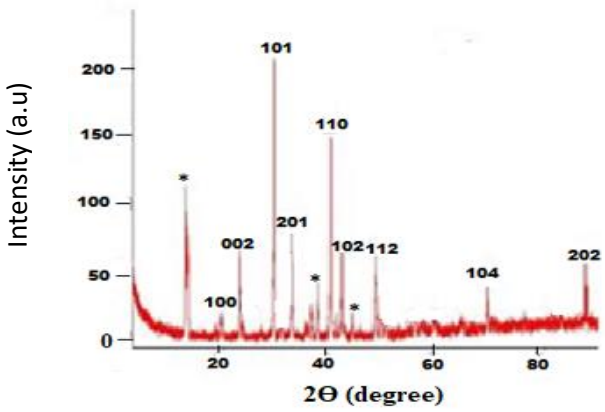

Figure 4.4: The XRD pattern of CdS nanoparticles from cadmium thiourea.

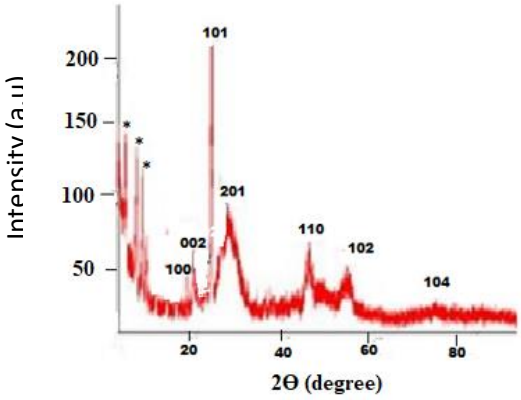

Figure 4.5: The XRD pattern of CdS nanoparticles from cadmium thiourea*.

XRD patterns on **Figure 4.5** shows the mixture of hexagonal and cubic phase nanoparticles with the predominance of cubic phase represented by broad peaks around 30°, 45°, 50° and 80° 2 theta, representing 111, 220, 311 and 331 planes. The hexagonal phase is represented by 100, 002 and 101 planes with sharp peaks around 25°. The observed narrow peak (002) indicates that the particles are elongated towards the C-axis, which is the characteristics of wire or rod-shaped nanoparticles. The sharp and broad peaks on the pattern on **Figure 4.5** indicate different size distribution of nanoparticles with smaller size dominance since cubic phase broad particle are dominant.

TEM image is another useful tool in the characterization of nanoparticles for observation of the size and shape of the synthesized nanoparticles. The TEM images also show the particle distribution that gives the insight of the morphology of particles.

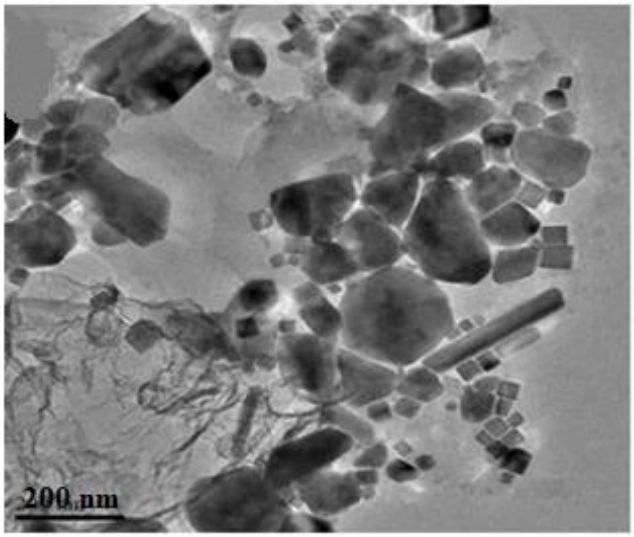

Figure 4.6: The TEM image of CdS nanoparticles from cadmium thiourea.

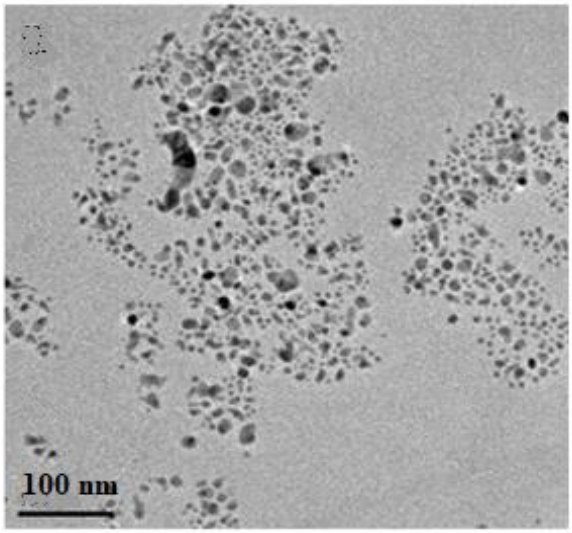

Figure 4.7: The TEM image of CdS nanoparticles from cadmium thiourea*.

Figure 4.6 and 4.7 represent the TEM images of CdS nanoparticles synthesized from single source precursor of cadmium thiourea complex and cadmium thiourea* using HDA as the capping agent and TOP as the solvent. **Figure 4.6** shows large particles with various sizes and are polydispersed with the dominance of cubic and rods shape particles, this TEM image confirms with the XRD patterns on **Figure 4.4** showing the hexagonal phase with sharp peaks presenting larger particles. UV-VIS spectrum of this CdS nanoparticles is blue shifted, which is also the confirmation of the formation of the nanoparticle. E. Morifi reported on the synthesis of CdS nanoparticles and he found similar arrangements of poly-dispersed and agglomerated nanoparticles of CdS, he reported that the agglomeration and poly-dispersity of nanoparticles

can be due to the different factors such as temperature, reaction time, capping agent nature, and concentration of precursor (Morifi,. 2014). **Figure 4.7** shows small particles size ranging from less than 50 nm, and the particles are poly dispersed with the predominance of spherical nanoparticles and the poly dispersity of the nanoparticles is also confirmed by XRD pattern on **Figure 4.5** which shows broad and sharp peaks which represent different particle size and shape.

(c) Optical properties of CdO nanoparticles.

Nanowires and nanofilms of cadmium oxide were previously synthesized using co-precipitation and sonochemical methods. Tabatabae et al. also reported on a simple method for synthesis of cadmium oxide nanoparticles by decomposition of Cd $(NO_3)_2.4H_2O$ in polyethylene glycol, and they reported that this approach directly forms the nanosized CdO (Tabatabaee *et al.*, 2013).

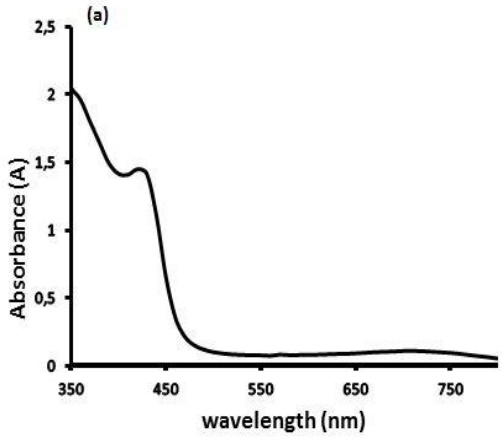

Figure 4.8: Absorption spectrum of CdO nanoparticles from cadmium urea complex.

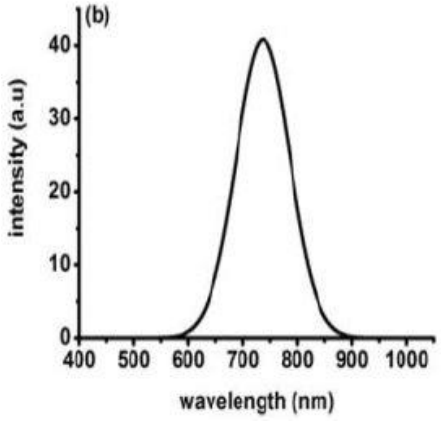

Figure 4.9: Emission spectrum of CdO nanoparticles from cadmium urea complex.

The optical absorption spectrum and emission fluorescence spectrum of CdO nanoparticles synthesized from cadmium urea precursor shown in **Figure 4.8 and 4.9** The absorption maximum blue shifted to 450 nm, as compared to the bulk band gap of 539 nm. This is an indication of presence of CdO particles with size below the bulk exciton dimension of cadmium oxide, Ghosh and co-workers reported that the bulk exciton Bohr radius of CdO is not available in the literature and is difficult to conclude to which confinement regime the CdO nanocrystals belongs (Ghosh et al., 2005). The maximum absorption observed in the spectrum of CdO nanoparticles is attributed to the lowest electronic transition occurring between conduction and valence band of CdO nanocrystallites. The resulting Fluorescence spectrum of CdO nanoparticles is shown in **Figure 4.9**. The fluorescence spectra of the sample show narrow emission peaks. The emission maximum is located at 750 nm, with maximum absorption been at 450 nm, this results in the stoke shift of 300 nm. From the blue shift on absorption spectrum on **Figure 4.8** we can conclude that the CdO nanoparticles were successfully synthesized by simple single source precursor method.

(d) CdO nanoparticles structural properties

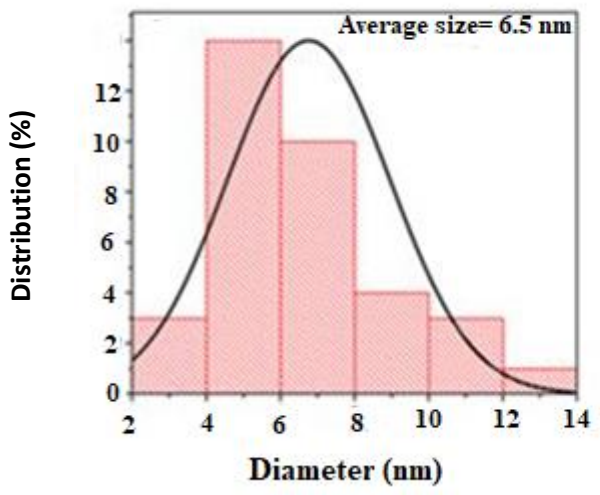

Figure 4.10: Histogram of CdO nanoparticles prepared from Cd-urea complex.

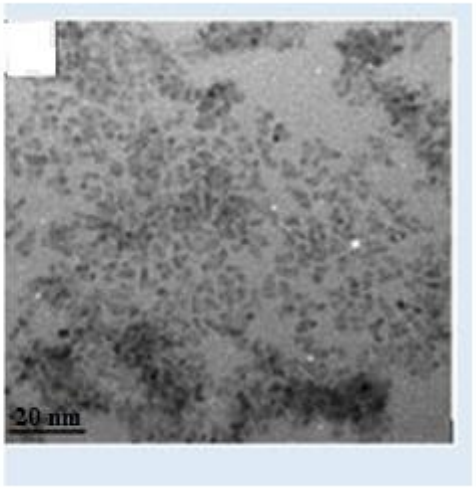

Figure **4.11**: TEM image of CdO nanoparticles prepared from Cd-urea complex

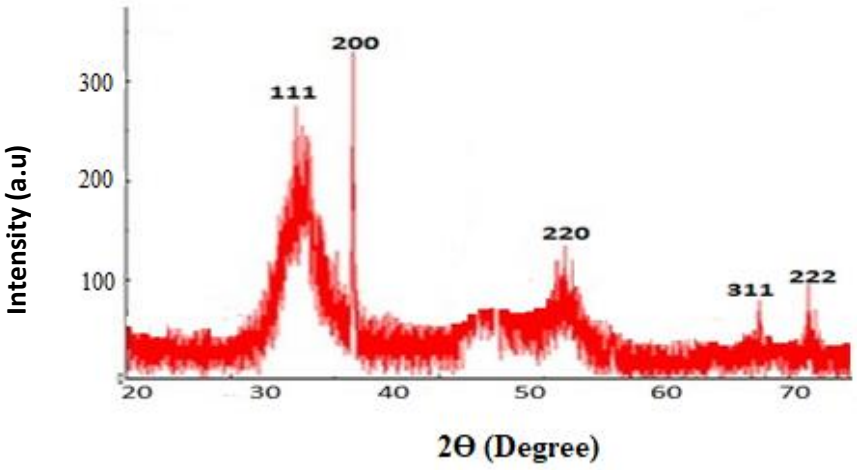

Figure 4.12: XRD pattern of CdO nanoparticles from Cd-urea.

Figure 4.11 show the TEM CdO nanoparticles synthesis from cadmium urea precursor. The TEM image shows that the CdO nanocrystallites are almost spherical in shape and largely monodispersed. The narrow emission peaks on **Figure 4.9** also confirm the small size distributions and the presence of anisotropic particle as they can be observed on the histogram

on **Figure 4.10** that the nanoparticles are largely mono-dispersed. Also, the large stoke shift on the emission fluorescence can be the indication of the small size distribution of CdO nanoparticles as the radius of nanoparticles decrease, thus the stoke shift increase. The Histogram shows the particle size average of 6.8 nm, and the particle size is ranging from 14-2 nm with the domination of particles between 4-6 nm. Morefi also reported on the same work of synthesis of CdO nanoparticles, using single source precursor method and cadmium urea as the precursor complex. The CdO nanoparticles possessed a cubic structure. The XRD patterns of CdO on **Figure 4.12** show the cubic phase nanoparticles with the existence of broad peak indexed (111 and 202) which indicates small particle size distribution. The peak indexed (200), (311) and (222) are narrow, showing the existence of the larger particles, even there is no observation of larger particles from the TEM images.

4.4.2 NiS and NiO nanoparticles from Ni-thiourea, nickel thiourea* and Ni-urea

(a) NiO nanoparticles Optical properties

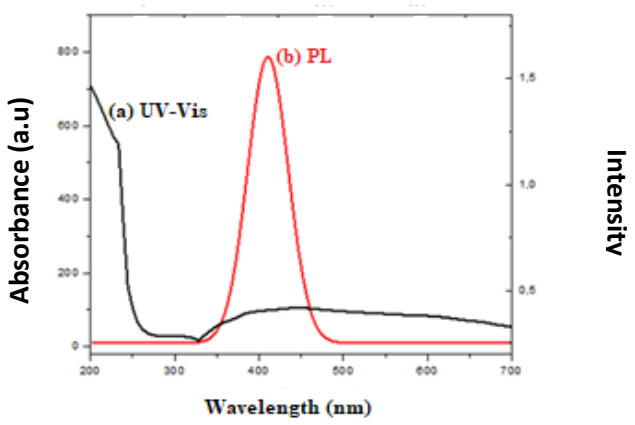

Figure 4.13: UV–vis spectra and PL of NiO nanoparticle.

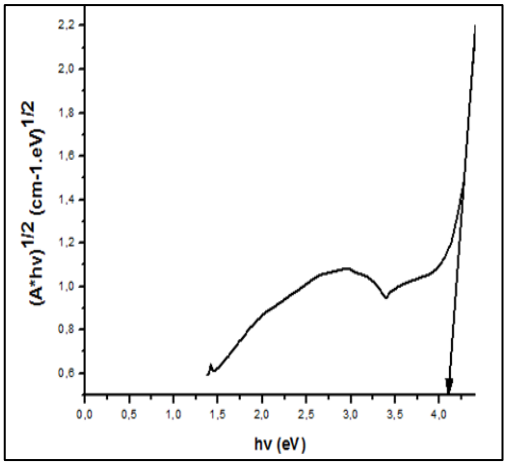

Figure 4.14: Talc plot spectra for NiO Nanoparticles.

Figure 4.13 shows the absorption band edge of NiO nanoparticles (270 nm) synthesized from single source precursor of nickel urea complex. This blue shift of the absorption edges from the bulk NiO particles is related to the size decrease of particles due to the quantum

confinement effect of the nanoparticles. The emission spectrum of NiO nanoparticles is also shown in **Figure 4.13.** The maximum emission peak is red-shifted from the maximum absorption peak of NiO nanoparticles with the stoke shift of 150 nm. It is necessary to mention that the optical direct band gap values of the NiO samples were determined by Tauc's relation (Barakat *et al.*, 2013):

$$\alpha h\nu = \alpha_0 (h\nu - E_g)^n \quad \text{(Equation 4. 1)}$$

Where hν, α_0, Eg and n are photon energy, a constant, optical band gap of the nanoparticles, and transition type respectively. Absorption coefficient (α) of the powders at different wavelengths can be calculated from the absorption spectra. The band gap of NiO nanoparticles is 4.5 eV, which is high than that of bulk NiO (3.74 eV) .From the UV-Vis band, energy shift from that of the bulk material NiO energy and PL shift it can be concluded that the NiO nanoparticles were synthesized successfully. This is further supported by TEM images and the XRD patterns of NiO synthesized nanoparticles.

(b) NiO nanoparticles structural properties

The structural properties of the NiO nanoparticles were further characterized by TEM to establish the size, morphology and the crystallinity of the particles. The TEM image in **Figure 4.15** confirm the nanosized and the almost spherical morphology of the nanoparticles. The existence of other morphology rather than spherical can be observed from the image. It has been previously reported that the single-source precursor method gives particles with relatively good dispersity.

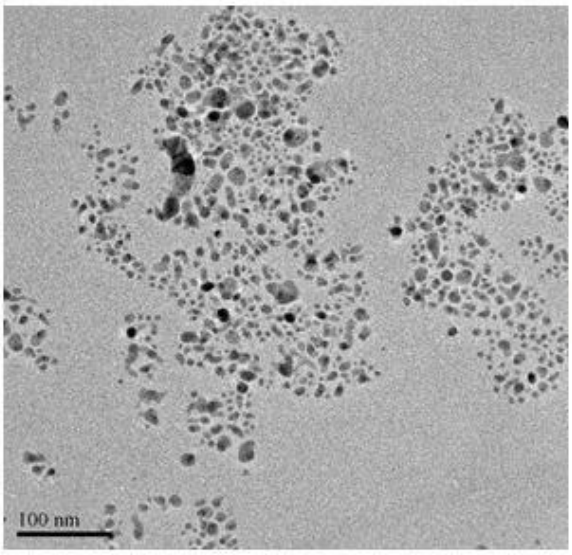

Figure 4.15: TEM image of NiO nanoparticles prepared from Ni-urea complex.

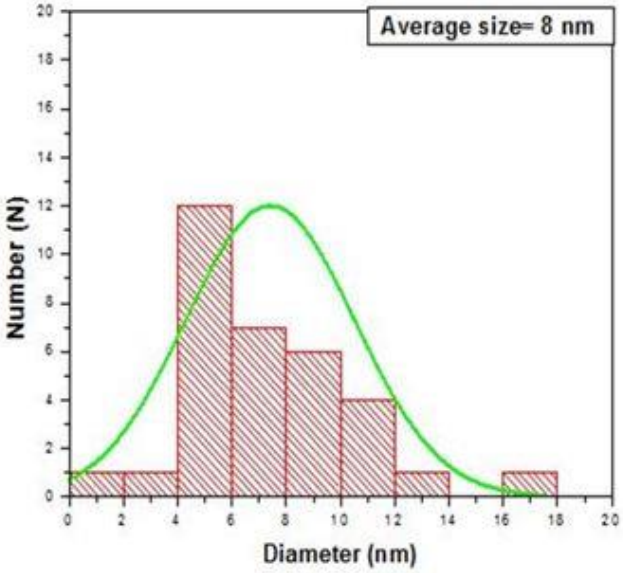

Figure 4.16: Histogram of NiO nanoparticles prepared from Ni-urea complex.

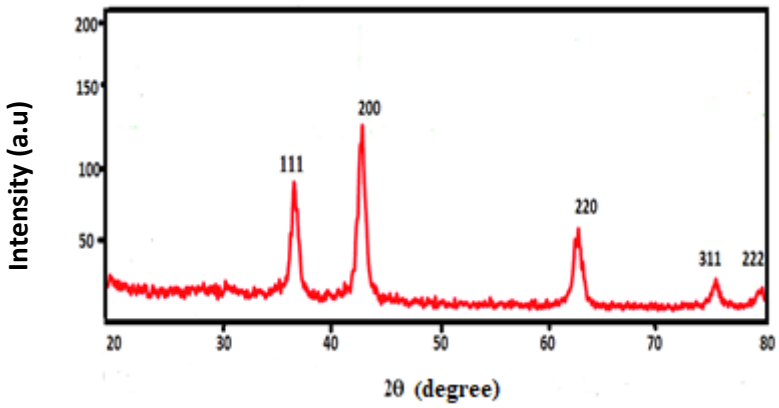

Figure 4.17: XRD pattern of NiO nanoparticles prepared from Ni-urea complex.

The histogram in **Figure 4.16** shows the average particle size of 8 nm, with the domination of particle size between 4-6 nm. **Figure 4.17** shows the XRD pattern of the NiO nanoparticles prepared by single source precursor of Ni-urea complex. The powders showed a crystalline pattern. According to the standard NiO pattern [JCPDS: 75-0197], all diffraction peaks can be well indexed as face-centered cubic phase at about $2\theta = 37.27$ 43.2978, 62.86, 75.63, and 79.60 which are assignable to (111), (200), (220), (311), and (222) crystal planes, respectively.

(c) Qualitative analysis and optical properties of NiS nanoparticles

Nickel sulfide bulk material is a p-type semiconductor with a band gap of 0.5 eV (Saeed and Rashid, 2015). The phase diagram of the Ni–S system is more complex than that of iron and cobalt sulfides, making it a less studied material compare to other semiconducting metal chalcogenides. The complexity of NiS is due to the valence electronic configuration of nickel ($3d^8 4S^2$) and making NiS form more than one crystalline phases with sulfur. Crystalline phases and stoichiometries like Ni_3S_2, Ni_6S_5, Ni_7S_6, Ni_9S_8, NiS, Ni_3S_4, and NiS_2 have been reported by Barry and Ford, synthesized using other methods rather than single source precursor method. The single source precursor method has been previously used or reported extensively for the synthesis of nickel sulfide thin films via CVD method (Saeed and Rashid, 2015). Roffey reported on the synthesis of α-NiS in oleylamine at 230 °C, using single source precursor method (Roffey *et al.*, 2016).

Figure 4.18 shows the absorption and emission spectrum of NiS nanoparticles synthesized at 160 °C from single source nickel thiourea precursor using HDA as the capping agent. The UV-Vis spectrum shows the strong blue shift of the band edge to 300 nm from 620 nm of the bulk NiS. The strong blue shift was due to strong confinement effect as the NiS nanocrystals become very small compared to the Bohr exciton radius.

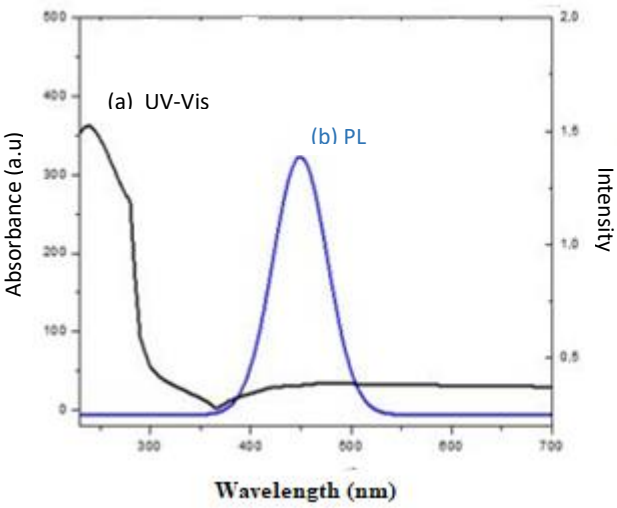

Figure 4.18: The UV-Vis and PL spectra of NiS Nanoparticles synthesized from Ni-thiourea nanoparticles.

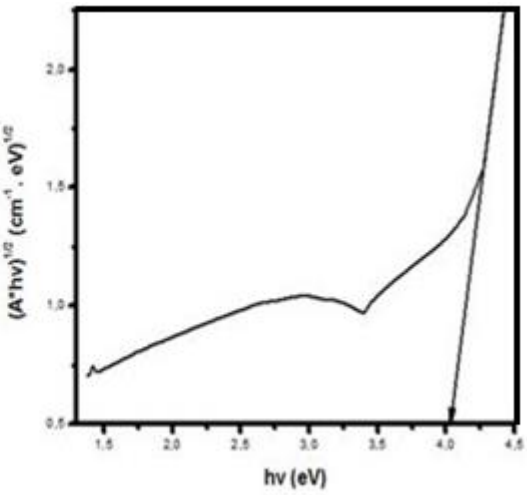

Figure 4.19: Talc plot of NiS Nanoparticles synthesized from Ni-thiourea nanoparticles

The energy level within the electronic structure of the nickel sulfide becomes quantize and results in the blue shift of the band-gap. The fluorescence emission spectrum is shown in **Figure 4.18** and it gives the maximum emission peak is red-shifted with the stoke shift of 150 nm from the maximum absorption peak. The blue shift and red shift of absorption peak and emission peak indicate the formation of NiS nanoparticles from thermal decomposition of the single source precursor of nickel thiourea in HDA at 160 °C. The Talc plot is shown in **Figure 4.19** indicates higher energy of 4.0 eV compare to the energy of bulk material of NiS. This increased in energy as the semiconductors particles are turned to smaller size, makes this material have a great potential application in much different real life situations.

(d) NiS nanoparticles structural properties

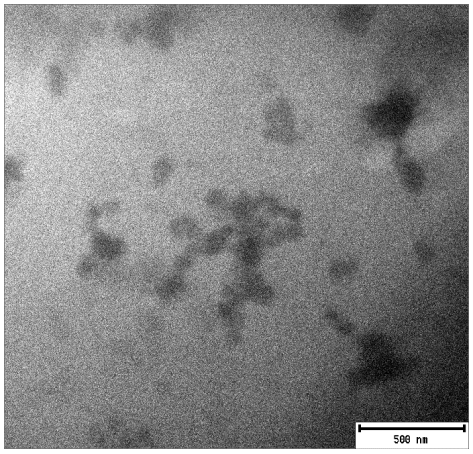

Figure 4.20: TEM images of NiS nanoparticles from Ni-thiourea complex.

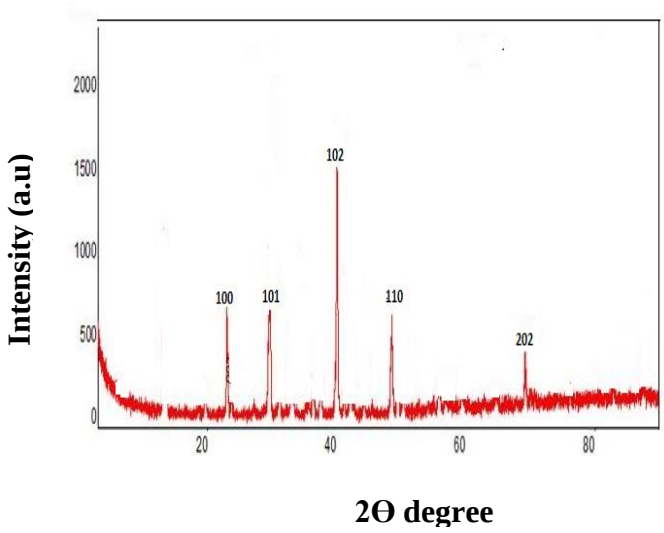

Figure 4.21: XRD pattern of NiS nanoparticles from Ni-thiourea complex.

The TEM image in **Figure 4.20** shows the NiS nanoparticles. The particles were agglomeration, with no clear morphology. A cluster of particles can be observed from the TEM images, making it difficult to determine the particles size and shape. The XRD patterns on **Figure 4.21** shows the hexagonal NiS nanoparticles.

The NiS nanoparticles were also synthesized on other experiment using nickel thiourea* to evaluate the properties of NiS nanoparticles from nickel thiourea*. The synthesized NiS nanoparticles were compared to those synthesized from nickel thiourea complex, to investigate the effect of the nature of the synthesized complex on the properties of the nanoparticles.

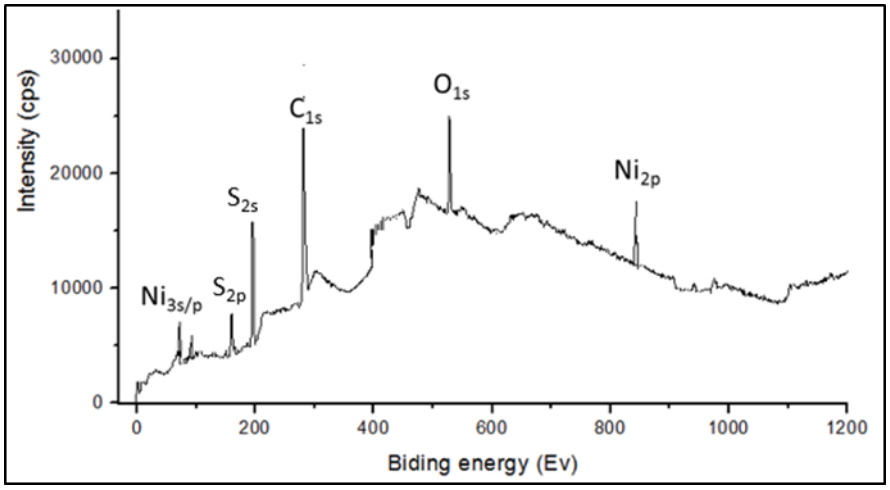

Figure 4.22: X-ray photoelectron spectrum of nanoparticles from nickel thiorea*.

Figure 4.22 present the XPS survey spectra of the NiS particles from nickel thiourea* with all the binding energies calibrated using C 1s (284 eV). The spectrum provides information on the existence of Ni, S and O elements in the sample. The peaks of C and O were related to reference and absorbed gaseous molecules on the exposure of the sample to atmospheric air. The only difference from CdS XPS spectrum is the substitution of the Cd 3d binding energies by Ni 2s binding energy at 845 eV. The two peaks at around 200 eV are probably due to S 2p and S 2s transitions are also present here. This XPS survey spectrum shows that the nanoparticles from this complex are of nickel sulfide. From this, it can be confirmed that this complex is nickel thiourea.

Figure 4.23 is the absorption and emission spectra of the NiS nanoparticles synthesized from nickel thiourea*. Absorption spectrum shows the blue shift of the wavelength to 300 nm from the wavelength of 630 nm bulk NiS materials. This shift is now well-known to be due to the decrease in the size of the particles of the bulk material to the nanosized materials. The emission spectrum shows the red shift of the maximum peak from the absorption maximum peak, with the stoke shift of 150 nm.

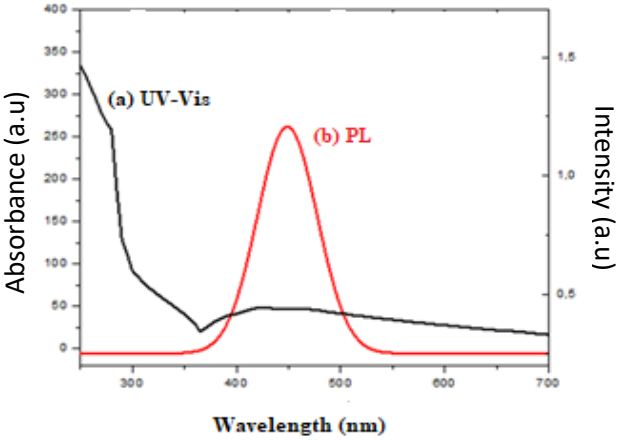

Figure 4.23: UV-vis and PL spectra of NiS nanoparticles from nickel thiourea*.

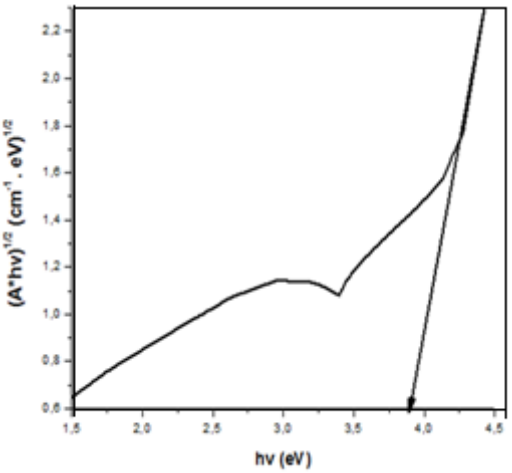

Figure 4.24: Talc plot of NiS nanoparticles from nickel thiourea*.

The TEM images in **Figure 4.25** represent the HDA capped NiS nanoparticles synthesized from nickel thiourea*. Smaller particles were synthesized and this could be seen from the blue shift of wavelength from the UV-Vis spectrum and redshift of PL spectrum.

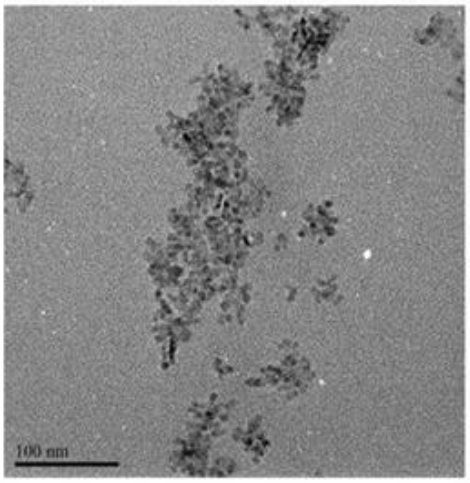

Figure 4.25: TEM image of NiS nanoparticles from nickel thiourea*.

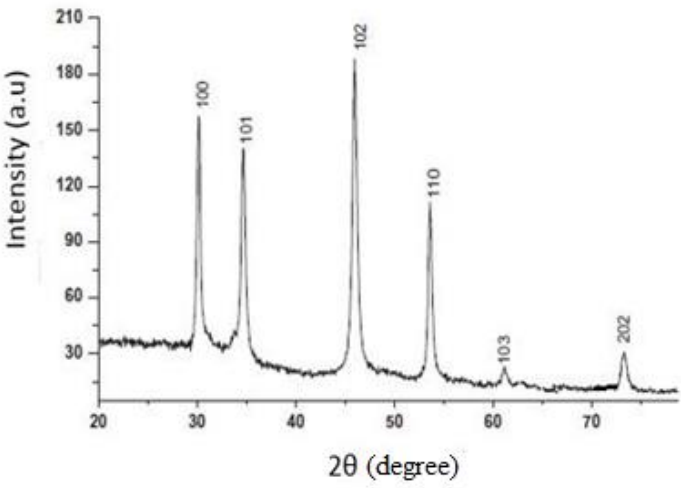

Figure 4.26: XRD patterns of NIS nanoparticles from nickel thiourea*.

From this TEM image, the spherical nanoparticles can be observed, these particles are conjugated into one area, making it difficult for clear observation of the nanoparticles morphology. The XRD pattern for this NiS nanocrystals shown in **Figure 4.26** the XRD pattern shows diffractions of hexagonal NiS and the space group P63/mmc with major diffraction peaks of (100), (101), (102) and (110) planes (ICDD: 075-0613).

Chapter 05

Overall conclusion and recommendations

5.1 Conclusion

Thiourea and urea complexes of cadmium and nickel were successfully synthesized and used as single source precursors for the preparation of cadmium and nickel chalcogenide nanoparticles. Various analytical techniques such as FTIR and TGA were used to characterize the complexes. The metal thiourea complexes were found to be coordinating with the center metal through the sulfur atom and the metal urea complexes through the oxygen atom. The synthesized metal complexes were further used as a single source precursors for the synthesis of metal sulfide and oxide nanoparticles using single source precursor method. The advantage of these complexes in their application for the synthesis of metal chalcogenide nanoparticles is that, the bond between the metal and the chalcogen already exist, and thermalize of this complexes under optimum parameters lead to the formation of metal chalcogenide nanoparticles.

Cadmium thiourea* complex showed the same properties or characteristics as those of cadmium thiourea and nickel thiourea* also showed same properties as those of nickel thiourea complex. This similarity of characteristics was observed from the FTIR spectroscopy, elemental analyses and TGA. A combined use of analytical data of elemental analysis, FTIR and TGA provides not only complimentary but also confirmatory data to unambiguously and correctly formulate of the synthesized complexes as the metal sulfides complexes, not the thiourea-urea metal complexesl. The synthesized complexes were stable under normal conditions to be used for the synthesis of the nanoparticles. All the complexes showed major decomposition stage at around 200 °C, and the decomposition below this temperature was assigned to the loss of water (at 100 °C) and another solvents like methanol or methanol used to wash the complexes.

UV-Vis spectroscopy of the synthesized metal chalcogenide nanomaterials showed that they were blue shifted compared to their bulk materials absorption wavelength, indicating that the semiconductor metal chalcogenide nanoparticles were successfully synthesized from metal thiourea and urea complexes.

Cadmium sulfide nanoparticles were synthesized from cadmium thiourea complex and their absorption spectroscopy was shifted to 475 nm, bulk CdS absorb light at 515 nm. The PL spectroscopy maximum peak was red-shifted with the stoke shift of 80 nm from the absorption maximum peak. Also, the nanoparticles from cadmium thiourea* were those of CdS. The CdS nanoparticles from cadmium thiourea and cadmium thiourea complex showed more similarities also on their optical. Cadmium sulfide nanoparticles from cadmium thiourea showed the hexagonal phase in their XRD patterns with large size distribution which is confirmed by TEM image of CdS nanoparticles. CdS nanoparticles were also successfully synthesized from cadmium thiourea*. The XRD of this CdS nanopartilces showed phases of cubic and hexagonal with sharp XRD peaks which indicated the distribution of small particles size, which can be observed from TEM image. Cadmium oxide nanoparticles were also successfully synthesized from cadmium urea complex by simple single source precursor method. The nanoparticles show no similarities from those from cadmium thiourea*. TEM image of CdO nanoparticles shows the small size particles distribution with the average particle size of 6.8 nm which is in confirmatory with CdO XRD patterns showing the very broad peaks.

Nickel chalcogenide semiconductor nanoparticles were also successfully synthesized by single source precursor method. The NiO nanoparticles showed the band edge shift of 270 nm, which is due to a decrease in size of particles. The emission maximum peak was red shifted from the absorption maximum peak with the stoke shift of 150 nm. NiS nanoparticles were also

successfully synthesized from nickel thiourea and nickel thiourea*. The XPS spectroscopy of NiS* nanoparticles shows the existence of Ni, S, O and C elements, in which carbon and oxygen can be assigned to reference and the gaseous substances absorbed from the atmospheric air.

5.2 Recommendations for future work

The synthesized complexes from the reaction of metal, Urea and thiourea resulted in the end product of metal thiourea complexes.

The following can be done to synthesize the ideal complex of thiourea-urea metal complex:

1. Use of other semiconducting metals that has high affinity for both sulfur and oxygen.
2. Study of the affinity of other chalcogenides e.g. tellurium and selenium.

Other chalcogenides, like selenium and tellurium can also be explored for the synthesis of cadmium and nickel dichalcogenides materials containing selenium and sulphur or oxygen and tellurium.

REFERENCES

AHMED, L. A., MOHAMMAD, A. M. and OBRIEN, P., 2012. High-throughput route to CuS nanoparticles from single molecular precursor, *Material science in semiconductor processing*, 1**5**, pp. 218-221.

AL-HADA, N. M., SAION, E. B., SHAARI, A. H., KAMARUDIN, M.A., FLAIFEL, M. H., AHMAD, S. H. and GENE, A., 2014. A facile thermal-treatment route to synthesize the semiconductor CdO nanoparticles and effect of calcinations, *Material science in semiconductor processing*, **26**, pp. 460-466.

ALKAN, C., TEK, Y. and KAHRAMAN, D., 2011. Preparation and characterization of a series of thiourea derivatives as phase change materials for thermal energy storage, *Turkish Journal of Chemistry*, **35**, pp. 769–777.

AMBUJAM, K., THOMAS, P. C., ARUNA, S., ANAND, D. P. and SAGAYARAJ, P., 2007. Study of Optical, Electrical, and Magnetic Properties of Tetrakis Thiourea Nickel Chloride Single Crystals, *Materials and Manufacturing Processes*, **22**, pp. 346–350.

BAO, S. J., LI, Y., LI, C. M., BAO, Q., LU, Q. and GUO, J., 2008. Shape evolution and magnetic properties of cobalt sulfide, *Cryst. Growth Des*, **8**, pp 3745–3749.

BARAKAT, A., AL-NOAIMI, M., SULEIMAN, M., ALDWAYYAN, A. S., HAMMOUTI, B., HADDA, T. BEN, HADDAD, S. F., BOSHAALA, A. and WARAD, I., 2013. One step synthesis of NiO nanoparticles via solid-state thermal decomposition at low-temperature of novel aqua(2,9-dimethyl-1,10-phenanthroline)$NiCl_2$ complex, *International Journal of Molecular Sciences*, **14**, pp. 23941–23954.

BAWENDI, M. G., KAGAN, C. R. and MURRAY, C. B., 2000. Synthesis and characterization of monodisperse nanocrystals, *Annual Review of Material Science*, **610**, pp. 545-551.

BERA, P. and SEOK, S., 2012. Nanocrystalline copper sulfide of varying morphologies and

stoichiometries in a low temperature solvothermal process using a new single-source molecular precursor, *Solid State Sciences*. Elsevier Masson SAS, **14**, pp. 1126–1132.

BEREMAN, R. D., CHURCHILL, M. R. and SHIELDS, G., 1979. Coordination Chemistry of Sulfur-Containing Ligands, *Inorganic Chemistry*, **18**, pp. 3117–3121.

BISWAS, K. and RAO, C. N. R., 2007. Use of ionic liquids in the synthesis of nanocrystals and nanorods of Semiconducting metal chalcogenides, *Chem. Eur. J*, **13**, pp. 6123-6129.

BRUS. L. E., 1986. Electronic wave functions in semiconductor clusters: Experiment and theory, *J. Phys. Chem*, **90**, pp. 2555-2560.

CARROLL, K. J., HUDGINS, D. M., SPURGEON, S., KEMNER, K. M., MISHRA, B., BOYANOV, M. I., BROWN, L. W., TAHERI, M. L. and CARPENTER, E. E., 2010. One-pot aqueous synthesis of Fe and Ag core/shell nanoparticles, *Chemistry of Materials*, **22**, pp. 6291–6296.

CHANDRA, S., KUMAR, A. and TOMAR, P. K., 2014. Synthesis and characterization of copper nanoparticles by reducing agent', *Journal of Saudi Chemical Society*, **18**, pp. 149–153.

CHEN, M., XIE, Y., LU, J., XIONG, Y., ZHANG, S., QIAN, Y. T., and LIU, X., 2002. Synthesis of rod-, twinrod-, and tetrapod-shaped CdS nanocrystals using a highly oriented solvothermal recrystallization technique, *J. Mater. Chem*, **12**, pp. 748-753.

CHOWDHURY, S., AHMED, G. A., MOHANTA, D., DOLUI, S. K., AVASTHI, D. K., and CHOUDHURY, A., 2005. Luminescence study of bare and coated CdS quantum dots: Effect of SHI irradiation and ageing, *Nucl. Instr. Meth. Phys. Res. B*, **240**, pp. 690-696.

CHRISTIAN, P. and O'BRIEN, P., 2008. Thermodynamic and kinetic control of crystal growth in CdS nanomaterials, *J. Mater. Chem*, **18**, pp. 1689–1693.

CHUNGGAZE, M., JONES, A. C., MALIK, M. A., O'BRIEN, P., TRINDADE, T. and WALSH, J. R., 1997. Precursor chemistry: remaining challenges and some novel approaches,

Journal of crystal growth, **170**, pp. 23-29.

CLEMENS, R. and MAHENDRA, P., 2013. Biosynthesis of nanoparticles, *C.A.B Internationa issuing*, **01**, pp. 13-61.

CUSHING, B. L., KOLESNICHENKO, V. L. and O'CONNOR, C. J., 2004. Recent advances in the liquid-phase syntheses of inorganic nanoparticles, *Chemical Reviews*, **104**, pp. 3893–3946.

DARKWA, J., LITORJA, JR L. A., OSEI-TWUM, E.Y., and THOMAS, M. S., 1999. Synthesis characterisation and stability of mixed aryldichalcogenide bis(diphenylphosphino) ethane nickel (II) complexes, *Polyhedron*, **18**, pp. 2803-2810.

DERAKHSHI, M., JAMALI, T., ELYASI, M., BIJAD, M., SADEGHI, R., KAMALI, A., NIAZAZARI, K., SHAHMIRI, M. R., BAHARI, A. and MOKHTARI, S., 2013. Synthesis and characterization of NiO nanoparticle as a high sensitive voltammetric sensor for vitamin C determination in food samples, *International Journal of Electrochemical Science*, **8**, pp. 8252–8263.

DESHPANDE, M. P., PATEL, K. N., GUJARATI, V. P., PATEL, K. and CHAKI, S. H., 2016. Structural, Thermal and Optical Properties of Nickel Oxide (NiO) Nanoparticles Synthesized by Chemical Precipitation Method, *Advanced Materials Research*, **1141**, pp. 65–71.

DETHLEFSEN, J. R. and DØSSING, A., 2011. Preparation of a ZnS shell on CdSe quantum dots using a single-molecular ZnS precursor, *Nano Letters*, **11**, pp. 1964–1969.

DHANAM, M., DEVASIA, D. P., KAVITHA, B. and MAHESWARI B., 2010. Structural and optical analysis of CdS nanocrystals prepared by low temperature thermolysis, *Dig. J. Nanomater. Biostruct*, **5**, pp. 587-592.

DUTTA, D. P., SHARMA, G. and GOPALAKRISHNAN, I. K., 2008. Single molecular precursor route to nanocrystalline jaipurite: synthesis, characterization and magnetic

property, *Mater. Lett*, **62**, pp. 1275–1278.

EL-NAHHAS, M. M., ABDEL-KHALEK, H. and SALEM, E., 2012. Structural and Optical Properties of Nanocrystalline 3,4,9,10-Perylene-Tetracarboxylic-Diimide Thin Film, *Advances in Condensed Matter Physics*, **20**, pp. 1–7.

FAN, D., AFZAAL, M., MALIK, M. A., NGUYEN, C. Q., O'BRIEN, P. and THOMAS, P. J., 2007. Using coordination chemistry to develop new routes to semiconductor and other materials, *Coord. Chem. Rev*, **251**, pp. 1878–1888.

FARAMARZ, F., JORGE, P., MARTINS, M. A., SANTOS, J. S. and TRINDADE, T., 2007. Fiber sensing using quantum dots, *Sensor (Basel)*, **12**, pp. 3489-3534.

FEYMAN, R. P., 1959. There is plenty of room at the bottom. T*he transcript of a talk*, pp. 01-08.

FLIEDEL, C. and BRAUNSTEIN, P., 2014. Recent advances in S-functionalized N-heterocyclic carbene ligands: From the synthesis of azolium salts and metal complexes to applications, *Journal of Organometallic Chemistry*. Elsevier B.V, **751**, pp. 286–300.

FREITAS, R. A., 2005. What is nanomedicine?, *Nanomedicine: Nanotechnology, Biology, and Medicine*, **1**, pp. 2–9.

GAO, F., LU, Q. Y., XIE, S. H., and ZHAO, D. Y., 2002. A Simple route for the synthesis of multi-armed CdS nanorod-based materials, *Adv. Mater*, **14**, pp. 1537-1540.

GHEZELBASH, A. and KORGEL, B. A., 2005. Nickel sulfide and copper sulfide nanocrystal synthesis and polymorphism, *Langmuir*, **21**, pp. 9451–9456.

GHOSH, P. K., DAS, S. and CHATTOPADHYAY, K. K., 2005. Temperature dependent structural and optical properties of nanocrystallineCdO thin films deposited by sol-gel process, *Journal of Nanoparticle Research*, **7**, pp. 219–225.

GUO, L., CHEN, S. anf CHEN, L., 2007. Controllable synthesis of ZnS/PMMA nanocomposites hybrids generated from functionalized ZnS quantum dots nanocrystals,

Colloid Polym. *Sci*, **285**, pp. 1593-1600.

HUANG, Y., CHEN, Y., HU, C., ZHANG, B., SHEN, T., CHEN, X. AND ZHANG, M. Q., 2012. 'Bridge' effect of CdS nanoparticles in the interface of graphene–polyanilinen composites, *J. Mater. Chem*, **22**, pp. 10999–11002.

IBRAHIM, O. B., REFAT, M. S. and SALMAN, M., 2012. Chemical Studies on the Uses of Urea Complexes to Synthesize Compounds Having Electrical and Biological Applications, *International Journal of Material Science*, **2**, pp. 67–82.

JORGE, P., MARTINS, M. A., TRINDADE, T., SANTOS, J. L. and FARAHI, F., 2007. Optical Fiber Sensing Using Quantum Dots, *Sensors*, **7**, pp. 3489–3534.

JOSHI, S., 2004. Preparation and characterization of CdS nanoparticles, *Inorganic Chemistry Communications*, **15**, pp. 1522–1523.

JUN, Y., JUNG, Y. and CHEON, J., 2002. Architectural Control of Magnetic Semiconductor Nanocrystals, *Journal of the American Chemical Society*, **124**, pp. 615–619.

KARTHIKEYAN, R., THANGARAJU, D., PRAKASH, N. and HAYAKAWA, Y., 2015. Single-step synthesis and catalytic activity of structure-controlled nickel sulfide nanoparticles', *CrystEngComm*, **17**, pp. 5431–5439.

KASHIWABA, Y.; SATO, J. and ABE, T., 2003. Emission of lights of various colors from p-CdS: Cu/n-CdS thin-film diodes, *Appl. Surf. Sci*, **212**, pp. 162-165.

KEULEERS, R., PAPAEFSTATHIOU, G. S., RAPTOPOULOU, C. P., PERLEPES, S. P. and DESSEYN, H. O., 2000. Comparative study of the metal – ligand bond strength in Mn II / X / U complexes (X = Cl , Br , I ; U = urea), *Journal of Molecular Structure*, **525**, pp. 173–183.

KHATY N, T., SURAMWAR, N. V. and THAKARE, S. R., 2012. One pot synthesis of copper nanoparticles at room temperature and its catalytic activity, Arabian journal of chemistry, **01**, pp. 01-06.

KHITRICH, N. V., SEIFULLINA, I. I., NEFEDOV, S. E. and MAZEPA, A. V., 2006. Interaction between N,N,N′,N′-tetramethylthiuram disulfide and cobalt(II) salts: Dependence of the product composition and structure on the nature of the anion, *Russian Journal of Inorganic Chemistry*, **51**, pp. 1000–1008. d

KRUIS, F. E., FISSAN, H. and PELED, A., 1998. Synthesis of nanoparticles in the gas phase for electronic, optical and magnetic applications - A review, *Journal of Aerosol Science*, **29**, pp. 511–535.

KUMAR, H., BARMAN, P. B. and SINGH, R. R., 2014. Development of CdS, ZnS Quantum Dots and their Core/Shell Structures by wet chemical method, **5**, pp. 40–53.

LAHEWIL, A. S. Z., AL-DOURI, Y., HASHIM, U. and AHMED, N. M., 2013. Structural, Analysis and Optical Studies of Cadmium Sulfide Nanostructured, *Procedia Engineering*, **53**, pp. 217–224.

LAKOWICZ, J. R., 2006. Principles of Fluorescence Spectroscopy Principles of Fluorescence Spectroscopy, Principles of fluorescence spectroscopy, *Springer, New York, USA*, 3rd edn, 2006.

LA MER, V. K. and DINEGAR, R. H., 1950. Theory, production and mechanism of formation of monodispersed hydrosols, *J. Am. Chem. Soc*, **72**, pp. 4847-4852.

LEE, H. L., MOHAMMED, I. A., BELMAHI, M., ASSOUAR, M. B., RINNERT, H. and ALNOT, M., 2010. Thermal and optical properties of cds nanoparticles in thermotropic liquid crystal monomers, *Materials*, **3**, pp. 2069–2086.

LEE, S. M., CHO, S. N. and CHEON, J., 2003. Anisotropic shape control of colloidal inorganic nanocrystals, *Adv. Mater*. **15**, pp. 441–444.

LIU, B., WEI, S., XING, Y., LIU, D., SHI, Z., LIU, X., SUN, X., HOU, S. and SU, Z., 2010. Complex-surfactant-assisted hydrothermal synthesis and properties of hierarchical worm-like cobalt sulfide microtubes assembled by hexagonal nanoplates, *Chemistry - A European*

Journal, 16, pp. 6625–6631.

LI, Y., AFZAAL, M. and O'BRIEN, P., 2006. The synthesis of amine-capped magnetic (Fe, Mn, Co, Ni) oxide nanocrystals and their surface modification for aqueous dispersibility, J. Mater. Chem, **16**, pp. 2175–2180.

LOU, W., CHEN, M., WANG, X. and LIU, W., 2007. Synthesis of high-luminescent cadmium sulfide nanocrystallites by a novel single-source precursor route, *Materials Letters*, **61**, pp. 3612–3615.

LUTFI ABDELHADY, A., MALIK, M. A. and OBRIEN, P., 2012. High-throughput route to Cu 2-xS nanoparticles from single molecular precursor, *Materials Science in Semiconductor Processing*. Elsevier, **15**, pp. 218–221.

MANSUROGLU, D. S., ARSLAN, H., FLÖRKE, U., and KÜLCÜ, N., 2008. Synthesis and characterization of nickel and copper complexes with 2,2-diphenyl-N-(alkyl(ararbamothioyl) acetamide: The crystal structures of HL1 and cis-[Ni(L1)2], *Journal of Coordination Chemistry*, **61**, pp. 3134–3146

MALIK, M. A., CHUNGGAZE, M., TRINDADE, T., WALSH, J. R., JONES, A. C. and O'BRIEN, P., 1997. Precursor chemistry: remaining challenges and some novel approaches, *Journal of Crystal Growth*, **170**, pp. 23–29.

MATTHEW, S. S., WANG, J., JOHNSTON-PECK, A. C., OLDENBURG, A. L. and TRACY, J. B., 2010. Synthesis of Au(core)/Ag(shell) nanoparticles and their conversion to AuAg alloy nanoparticles, Material science and engineering, **11**, pp. 01-05.

MCAFEE, L., 2000. Infrared and Raman Spectra of Inorganic and Coordination Compounds. Part A: Theory and Applications in Inorganic Chemistry; Part B: Application in Coordination, Organometallic, and Bioinorganic Chemistry, 5th Edition, *Journal of Chemical Education*, **77**, p. 1122.

MILANOVIC, V. and BUCALINA, A., 2013. Position of the Countries in Nanotechnology

and Global Competitiveness, *Management - Journal for theory and practice of management*, **18**, pp. 69–79.

MOHAMMADYANI, D., HOSSEINI, S. A. and SADRNEZHAAD, S. K., 2012. Characterization of Nickel Oxide Nanoparticles Synthesized Via Rapid Microwave-Assisted Route, *International Journal of Modern Physics: Conference Series*, **5**, pp. 270–276.

MOLOTO, M. J., REVAPRASADU, N., KOLAWOLE, G. A., MALIK, M. A., MOTEVALLI, M. and MARY, Q., 2010. Synthesis and X-Ray Single Crystal Structures of Cadmium (II) Complexes: CdCl2[CS(NHCH3)2]2 and CdCl2(CS(NH2)NHC6H5)4 - Single Source Precursors to CdS Nanoparticles- Single Source Precursors to CdS Nanoparticles, *E-Journal of Chemistry*, **7**, pp. 1148–1155.

MOLOTO, N., MOLOTO, M. J., COVILLE, N. J. and SINHA RAY, S., 2009. Optical and structural characterization of nickel selenide nanoparticles synthesized by simple methods, *Journal of Crystal Growth*, **311**, pp. 3924–3932.

MOLOTO, N., RAY, S. S. and MOLOTO, M. J., 2008. A Facile Route for the Synthesis of Poly(N-vinylcarbazole) Manganese Sulphide Quantum Dots Nanocomposites with Enhanced Optical Properties, *Journal of Nanoscience and Nanotechnology*, **8**, pp. 6031–6037.

MOLOTO, N., REVAPRASADU, N., MUSETHA, P. L. and MOLOTO, M. J., 2009. The effect of precursor concentration, temperature and capping group on the morphology of CdS nanoparticles, *Journal of nanoscience and nanotechnology*, **9**, pp. 4760–4766.

MONDAL, A. K., SU, D., CHEN, S., SUN, B., LI, K. and WANG, G., 2014. A simple approach to prepare nickel hydroxide nanosheets for enhanced pseudocapacitive performance, *RSC Advances*, **4**, p. 19476.

MORTLAND, M. M., 1966. Urea Complexes With Montmorillonite: An Infrared Absorption Study, *Clay Minerals*, **6**, pp. 143–156.

MURRAY, C. B., NORRIS, D. J. and BAWENDI, M. G., 1993. Synthesis and

characterization of nearly monodisperse CdE (E = sulfur, selenium, tellurium) semiconductor nanocrystallites, *J. Am.Chem,* Soc **115**, pp. 8706–8715.

MURUGANANDAM, S., ANBALAGAN, G. and MURUGADOSS, G., 2013. Synthesis and structural, optical and thermal properties of CdS: Zn2+ nanoparticles, *Appl. Nanosci*, **11**, pp. 4-8.

NAIR, G. and SURVASE, S., 2014. Synthesis and characterization of Ni nanoparticles, *Material and Methods*, **3**, pp. 56–60.

NIELSEN, K. H. and PEDERSEN, T., 2004. Determining particle size of NiO nanoparticles, **19**, p. 2004.

ONWUDIWE, D. C., STRYDOM, C A. and OLUWAFEMI, O. S., 2013. Effect of some nitrogen donor ligands on the optical and structural properties of CdS nanoparticles, *New J. Chem*, **37**, pp. 834-842.

42. ONWUDIWE, D. C., STRYDOM, C. A., OLUWAFEMI, O. S., HOSTEN, E. and JORDAAN, A., 2014. Synthesis, spectral and thermal studies of pyridyl adducts of Zn(II) and Cd(II) dithiocarbamates, and their use as single source precursors for ZnS and CdS nanoparticles, *Dalton Trans*, **43**, pp. 8703-8712.

PABITHA, G. and DHANASEKARAN, R., 2007. Growth and Characterization of a Non Linear Optical Crystal -Bis Thiourea Cadmium Chloride, *International Journal of Innovative Research in Science, Engineering and Technology*, **3297**, pp. 34–38..

PARK, B., SOCIETY, R. and PARK, B., 2007. Current and Future Applications of Nanotechnology, Nanotechnology: Consequences for Human Health and the Environment, RM Harrison, RE Hester (Eds.), The Royal Society of Chemistry, **24**, pp. 1–18.

PENLAND, R. B., MIZUSHIMA, S., CURRAN, C. and QUAGLIANO, J. V., 1957. Infrared Absorption Spectra of Inorganic Coördination Complexes. X. Studies of Some Metal-Urea Complexes 1a, b, *Journal of the American Chemical Society*, **79**, pp. 1575–1578.

PENTIMALLI, M., ANTOLINI, F., BAUER, E. M., CAPITANI, D., DI LUCCIO, T. and VIEL, S., 2006. A solid state nuclear magnetic resonance study on the thermolytic synthesis of CdS nanoparticles in a polystyrene matrix, *Mater. Lett*, **60**, pp. 2657-2661.

PICKETT, N. L. and O'BRIEN, P., 2001. Syntheses of semiconductor nanoparticles using single-molecular precursors, *Chem. Rec*, **1**, pp. 467–479.

POLTE, J., 2015. Fundamental growth principles of colloidal metal nanoparticles – a new perspective, *CrystEngComm*. Royal Society of Chemistry, **17**, pp. 6809–6830.

POST, T., 2008. Growth and Characterization of a New Non-Linear Optical Crystal : Urea Thiourea Zinc Chloride, **20**, pp. 5067–5070.

POZNYAK, S. K., TALAPIN, D. V., SHEVCHENKO, E. V. and WELLER, H., 2004. Quantum dot chemiluminescence, *Nano Letters*, **4**, pp. 693–698.

PUSHPALATHA, H. L., BELLAPPA, S., NARAYANASWAMY, T. N. and GANESHA, R., 2014 Structural and optical properties of CdS thin film obtained by chemical bath deposition and effect of annealing, **52**, pp. 545–549.

QIAN, X., LI, Y., XIE, Y. and QIAN, Y., 2000 The synthesis and morphological control of nanocrystalline pyrite nickel disulfide and cobalt disulfide, *Mater. Chem. Phys* **66**, pp. 97–99.

QI, L., COLFEN, H. and ANTONIETTI, M., 2001. Synthesis and characterization of CdS nanoparticles stabilized by double-hydrophilic block copolymers. *Nano. Lett*, **1**, pp. 61-65.

RAHDAR, A., ALIAHMAD, M. and AZIZI, Y., 2015. NiO Nanoparticles : Synthesis and Characterization, **5**, pp. 145–151.

RAMASAMY, K., MANEERPRAKORN, W., MALIK, M. A. and O'BRIEN, P., 2010. Single-molecule precursor-based approaches to cobalt sulphide nanostructures, *Philosophical Transactions of the Royal Society of London. Series A*, **368**, p. 4249.

RAO, C. N. R. and PISHARODY, K. P. R., 1976. Transition metal sulfides, *Prog. Solid State Chem*, **10**, pp. 207–270.

RAO, R. H. and KALAINATHAN, S., 2012. Spectroscopic investigation, nucleation, growth, optical, thermal and second harmonic studies of novel semi-organic nonlinear optical crystal-Thiourea urea zinc sulfate, *Spectrochimica Acta - Part A: Molecular and Biomolecular Spectroscopy*. Elsevier B.V, **97**, pp. 456–463.

Rengaraj, S., Venkataraj, S., Jee, S. H., Kim, Y., Tai, C. W., Repo, E., Koistinen, A., Ferancova, A. and Sillanp, M., 2010. Cauliflower-like CdS microspheres composed of nanocrystals and their physicochemical properties, *Langmuir*, **27**, pp. 352–358

REVAPRASADU, N. and MLONDO, S. N., 2006. Use of metal complexes to synthesize semiconductor nanoparticles, *Pure and Applied Chemistry*, **78**, pp. 1691–1702.

RODRI´GUEZ-FRAGOSO, P., DE LA CRUZ, G. G., TOMA, S. A., MENDOZA-ALVAREZ, J. G. and ANGEL Z. O., 2010. Photoluminescence of CdS nanoparticles embedded in a starch matrix, *J. Lumin*, **130**, pp. 1128-1133

ROFFEY, A., HOLLINGSWORTH, N., ISLAM, H.-U., MERCY, M., SANKAR, G., CATLOW, C. R. A., HOGARTH, G. and DE LEEUW, N. H., 2016. Phase control during the synthesis of nickel sulfide nanoparticles from dithiocarbamate precursors, *Nanoscale*, **821**, pp. 11067–11075.

ROHWER, L. E. S., AND MARTIN, J. E., 2007. Luminescence decay of broadband emission from CdS quantum dots, *J. Lumin*, **127**, pp. 499-507.

SAEED, S. and RASHID, N., 2015. Growth and characterization of semiconducting nickel sulfide nanocrystals from air-stable single-source metal organic precursors, *Cogent Chemistry*. Cogent, **1**, pp. 1–9.

SAGADEVAN, S. and VEERALAKSHMI, A., 2014. Synthesis , Structural , and Dielectric Characterization of Cadmium Oxide Nanoparticles, *Annual Review of Materials Research,* **8**, pp. 1492–1495.

SAHOO, S. K. and LABHASETWAR, V., 2003. Nanotech approaches to drug delivery and

imaging, *Drug Discovery Today*, **8**, pp. 1112–1120.

SAIKIA, D., SAIKIA, P. K., GOGOI, M. R., SENGUPTA, P. and SHELKE, M. V., 2011. Synthesis and characterization of CdS/PVA nanocomposite thin films from a complexing agent free system, *Mater. Chem. Phys*, **131**, pp. 223-229.

SHEA, C. M., 2005. Future management research directions in nanotechnology: A case study, *Journal of Engineering and Technology Management - JET-M*, **22**, pp. 185–200.

SHORE, M. S., WANG, J., JOHNSTON-PECK, A. C., OLDENBURG, A. L. and TRACY, J. B., 2011. Synthesis of Au(core)/Ag(shell) nanoparticles and their conversion to AuAg alloy nanoparticles, *Small*, **7**, pp. 230–234.

SKOLNICK, M. S. and MOWBRAY, D. J., 2004. SELF-ASSEMBLED SEMICONDUCTOR QUANTUM DOTS: Fundamental Physics and Device Applications, *Annual Review of Materials Research*, **34**, pp. 181–218.

SONAWANE, M. S., SHINDE, M. S. and PATIL, R. S., 2015. Characterization of nickel sulphide thin films prepared by modified chemical method, *Indian Journal of Pure and Applied Physics*, **53**, pp. 686–690.

SRINIVASAN, B. R., NAIK, T. A., TYLCZYŃSKI, Z. and PRIOLKAR, K. R., 2014. Reinvestigation of growth of thiourea urea zinc sulfate crystal, *Spectrochimica Acta - Part A: Molecular and Biomolecular Spectroscopy*, **117**, pp. 805–809.

Srinivasan, N., 2014. Synthesis and characterization of functionalized dithiocarbamates: New single-source precursors for CdS, *Superlattices and Microstructures*. Elsevier Ltd, **65**, pp. 227–239.

SRIVASTAVA, P. and SINGH, K., 2012. Synthesis of CdSe nanoparticles by solvothermal route: Structural, optical and spectroscopic properties, *Advanced Materials Letters*, **3**, pp. 340–344.

SU, B. and CHOY, K. L., 2000. Microstructure and properties of the CdS thin films prepared

by electrostatic spray assisted vapour deposition (ESAVD) method, *Thin Solid Films*, **359**, pp. 160-164.

TABATABAEE, M., MOZAFARI, A. A., GHASSEMZADEH, M., NATEGHI, M. R. and ABEDINI, I., 2013. A Simple Method for Synthesis of Cadmium Oxide Nanoparticles Using Polyethylene Glycol, **45**, pp. 90–92.

TAMBORRA, M., STRICCOLI, M., COMPARELLI, R., CURRI, M. L., PETRELLA, A. and AGOSTIAN A., 2004. Optical properties of hybrid composites based on highly luminescent CdS nanocrystals in polymer, *Nanotechnology*, S240-S244.

TERANISHI, T., SARUYAMA, M. and KANEHARA, M., 2009. Seed-mediated synthesis of metal sulfide patchy nanoparticles, *Nanoscale*, **1**, p. 225.

THOMAS, M. S., DARKWA, J., OSEI-TWUM, E. Y. and LITORJA, L. A., 1999. Synthesis characterisation and stability of mixed aryldichalcogenide bis(diphenylphosphino)ethanenickel(II) complexes. X-ray structure of Ni(dppe)(SeC6H4S), *Polyhedron*, **18**, pp. 2803–2810.

TRINDADE, T., O'BRIEN, P. and PICKETT, N. L., 2001. Nanocrystalline semiconductors: Synthesis, properties, and perspectives, *Chemistry of Materials*, **13**, pp. 3843–3858.

TWENEY, R. D., 2006. Discovering Discovery: How Faraday Found the First Metallic Colloid, *Perspectives on Science*, **14**, pp. 97–121.

VALIZADEH, A. and MUSSA FARKHANI, S., 2014. Review: three synthesis methods of CdX (X = Se, S or Te) quantum dots, *IET Nanobiotechnology*, **8**, pp. 59–76.

VAN POPPEL, L. H., GROY, T. L. and CAUDLE, M. T., 2004. Carbon-Sulfur Bond Cleavage in Bis(N-alkyldithiocarbamato)cadmium(II) Complexes: Heterolytic Desulfurization Coupled to Topochemical Proton Transfer, *Inorganic Chemistry*, **43**, pp. 3180–3188.

VICTORIANO, L. I., 2000. The reactivity of metal species towards thiuram sulfides: an alternative route to the syntheses of metal dithiocarbamates, *Coordination Chemistry*

Reviews, **196**, p. 383.

VISWANATHAN, B**.**, 2008. Synthetic strategies in chemistry, **46**, pp. 1–361.

WANG, C., ZHANG, W., QIAN, X., ZHANG, X., XIE, Y. and QIAN, Y., 1999. An aqueous approach to ZnSe and CdSe semiconductor nanocrystals, *Materials Chemistry and Physics*, **60**, pp. 99–102.

WANG, D., ZHANG, Y. and CHEN, W., 2014. A novel nickel–thiourea–triethylamine complex adsorbed on graphitic C_3N_4 for low-cost solar hydrogen production, *Chemical Communications*, **50**, p. 1754.

WANG, G. Z. Z., WANG, Y. W. W., CHEN, W., LIANG, C. H. H., LI, G. H. H. and ZHANG, L. D. D., 2001. A facile synthesis route to CdS nanocrystals at room temperature, *Materials Letters*, **48**, pp. 269–272.

WANG, J., SOLLENBERGER, S. J., YUAN, Y., YOSENICK, T. J. and ADAIR, J. H., 2008. Silica Encapsulated CdS Tabular Nanocomposites via a Template Directed Agglomeration Mechanism, *Journal of Nanoscience and Nanotechnology*, **8**, pp. 5878–5886.

WANG, W., ZHANG, Q., ZHANG, B., LI, D., DONG, X., ZHANG, L. and CHANG, J., 2008. Preparation of monodisperse, superparamagnetic, luminescent, and multifunctional PGMA microspheres with amino-groups, *Chinese Science Bulletin*, **53**, pp. 1165–1170.

WANG, Y., ZHU, Q., TAO, L. and SU, X., 2011. Controlled-synthesis of NiS hierarchical hollow microspheres with different building blocks and their application in lithium batteries, *Journal of Materials Chemistry*, **21**, p. 9248.

WANG, Z., NAN, C., WANG, D. and LI, Y., 2014. Fabrication of 1D nickel sulfide nanocrystals with high capacitances and remarkable durability', *RSC Adv.*, **4**, pp. 47513–47516.

WINTER, J. O., GOMEZ, N., GATZERT, S., SCHMIDT, C. E. and KORGEL, B. A., 2004. Variation of cadmium sulfide nanoparticle size and photoluminescence intensity with altered

aqueous synthesis conditions, Colloids Surf. A: *Physicochem. Eng. Aspects*, **254**, pp. 147–157.

XING, N., XU, L. T., BAI, F. Y., SHAN, H., XING, Y. H. and SHI, Z., 2014. Synthesis and characterization of novel transition metal complexes with indole acetic acid ligands: Evaluation of their catalytic activity for the oxidation of cyclohexane, *Inorganica Chimica Acta*. Elsevier B.V., **409**, pp. 360–366.

XU, S., WANG, C. and CUI, Y., 2009. Influence of ligand and solvent on characters of ZnTe clusters, *Journal of Molecular Structure*. Elsevier B.V., **938**, pp. 133–136.

YAN, P. XIE, Y., QIAN Y. and LIU, X., 1999. A cluster growth route to quantum-confined CdS nanowires, *Chem. Commun*, **22**, pp. 1293-1294.

YANG, Y., CHEN, O., ANGERHOFER, A. and CAO, Y. C., 2008. On Doping CdS / ZnS Core / Shell Nanocrystals with Mn, *Growth Lakeland*, **130**, pp. 15649–15661.

YUE, G. H., YAN, P. X., FAN, X. Y., WANG, M. X., QU, D. M., WU, Z. G., LI, C. AND YAN, D. 2007. Structure and properties of cobalt disulfide nanowire arrays fabricated by electrodeposition. Electrochem. Solid State Lett, 10, pp. 29–31.

ZHANG, L. and WEBSTER, T. J., 2009. Nanotechnology and nanomaterials: Promises for improved tissue regeneration, *Nano Today*, **4**, pp. 66–80.

ZHANG, P., and GAO, L., 2003. Synthesis and characterization of CdS nanorods via hydrothermal microemulsion, *Langmuir*, **19**, pp. 208-2010.

ZHONG, X., LIU, S., ZHANG, Z., LI, L., WEI, Z. and KNOLL, W., 2004. Synthesis of high-quality CdS, ZnS, and Zn x Cd 1− x S nanocrystals using metal salts and elemental sulfur, *Journal of Materials Chemistry*, **14**, pp. 2790–2794.

ZHOU, H., LV, B., WU, D. and SUN, Y., 2012. Hydrothermal synthesis and characterization of NiS flower-like architectures, *Particuology*. Chinese Society of Particuology, **10**, pp. 783–788.

ZORKIPLI, N. N. M., KAUS, N. H. M. and MOHAMAD, A. A., 2016. Synthesis of NiO Nanoparticles through Sol-gel Method, *Procedia Chemistry*. Elsevier Ltd., **19**, pp. 626–631.